JGR Planets

RESEARCH ARTICLE
10.1029/2019JE006302

Postimpact Evolution of the Southern Hale Crater Ejecta, Mars

J. L. Collins-May[1], J. R. Carr[1], M. R. Balme[2], N. Ross[1], A. J. Russell[1], S. Brough[3], and C. Gallagher[4]

[1]Geography, Politics and Sociology, Newcastle University, Newcastle upon Tyne, UK, [2]School of Physical Sciences, The Open University, Milton Keynes, UK, [3]School of Environmental Sciences, University of Liverpool, Liverpool, UK, [4]UCD School of Geography, University College Dublin, Dublin, Ireland

Key Points:
- Ejecta deposits south of Hale crater exhibit a variety of previously undocumented landforms
- Ejecta surface morphology is the result of water incorporated into the ejecta, facilitating a diverse range of geomorphic processes
- Some landforms (e.g. mounds) may be unique to this region of Hale crater's ejecta

Correspondence to:
J. L. Collins-May,
j.collins-may@newcastle.ac.uk

Citation:
Collins-May, J. L., Carr, J. R., Balme, M. R., Ross, N., Russell, A. J., Brough, S., & Gallagher, C. (2020). Postimpact evolution of the southern Hale crater ejecta, Mars. *Journal of Geophysical Research: Planets*, *125*, e2019JE006302. https://doi.org/10.1029/2019JE006302

Received 2 DEC 2019
Accepted 8 AUG 2020
Accepted article online 18 AUG 2020

Abstract As one of the youngest large (>100 km wide) impacts on Mars, Hale crater offers a unique opportunity to observe well-preserved deposits of Mars' former interior. We utilize visible imagery (Context Camera [CTX] and High Resolution Imaging Science Experiment [HiRISE]) and elevation data (Mars Orbiter Laser Altimeter [MOLA], High Resolution Stereo Camera [HRSC], and HiRISE stereo pairs) to examine the region south of Hale crater, which contains the greatest density of landforms caused by with the impact. Linear depressions, mounds, and polygons indicate that the ejecta material contained volatiles and underwent substantial postimpact geomorphic evolution after it was emplaced. Ejecta landform formation was facilitated by volatiles, likely water ice displaced from the subsurface during the impact, contained within the material. We suggest that the ejecta flowed into valleys where it acted in a manner similar to terrestrial debris flows, leaving mounds, high-standing deposits, lobate flow margins, and fan structures. Continued flow and settling of the ejecta then caused deposit dewatering, producing networks of linear depressions, particularly in places where the flows of ejecta were constricted. However, these landforms are not present everywhere, and their formation was likely influenced by topography. This work highlights that, while volatiles were present over much of Hale crater's ejecta blanket, the surface expression of them is spatially variable on local and regional scales.

Plain Language Summary When meteorites hit Mars, material from underground is brought to the surface. The appearance of this material on the surface provides clues about the Martian subsurface. Given its size, Hale crater is young compared to other craters on Mars. This means that its deposits are better preserved and may hold more clues about their formation than older crater deposits. Detailed reconstructions of how these deposits changed over time tell us about the material they were originally made of and what was in the subsurface before Hale crater formed. This work provides the first detailed description of the ejecta deposits to the south of Hale crater and analyzes how features within the ejecta may have been created. The appearance of the Hale crater deposits suggests that the deposits once contained water, which most likely came from ice that was in the ground when the meteor that formed Hale crater impacted. In some locations, so much water was present in the Hale crater deposits that water flowed across the surface and carved channels, as well as formed mounds and cracked surfaces. However, these features are found only in certain locations, suggesting that the processes that formed them did not occur everywhere.

1. Introduction

Resolving the extent of water ice or other volatiles within the subsurface of Mars is a major research question, as it has biological and climatological implications for the present day and in the past (Carr, 1987). Direct observations of ice within fresh impact craters (Byrne et al., 2009), exposed scarps (Dundas et al., 2018), and holes excavated by the Phoenix lander (Mellon et al., 2009) indicate that frozen volatiles exist in the Martian subsurface. Multiple lines of evidence including gamma ray spectrometry (Boynton et al., 2002), neutron fluxes (Feldman et al., 2002), and radar data (Putzig et al., 2014) suggest that ground ice is widespread. This is supported by geomorphic features indicative of subsurface ice, such as thermokarst terrain (Soare et al., 2008), patterned ground (Mangold et al., 2004), and crater ejecta morphologies (Costard & Kargel, 1995). Despite this evidence, the global volumes and locations of ice in the Martian subsurface are still poorly constrained (Fanale et al., 1986). The Shallow Radar (SHARAD) and Mars Advanced Radar for

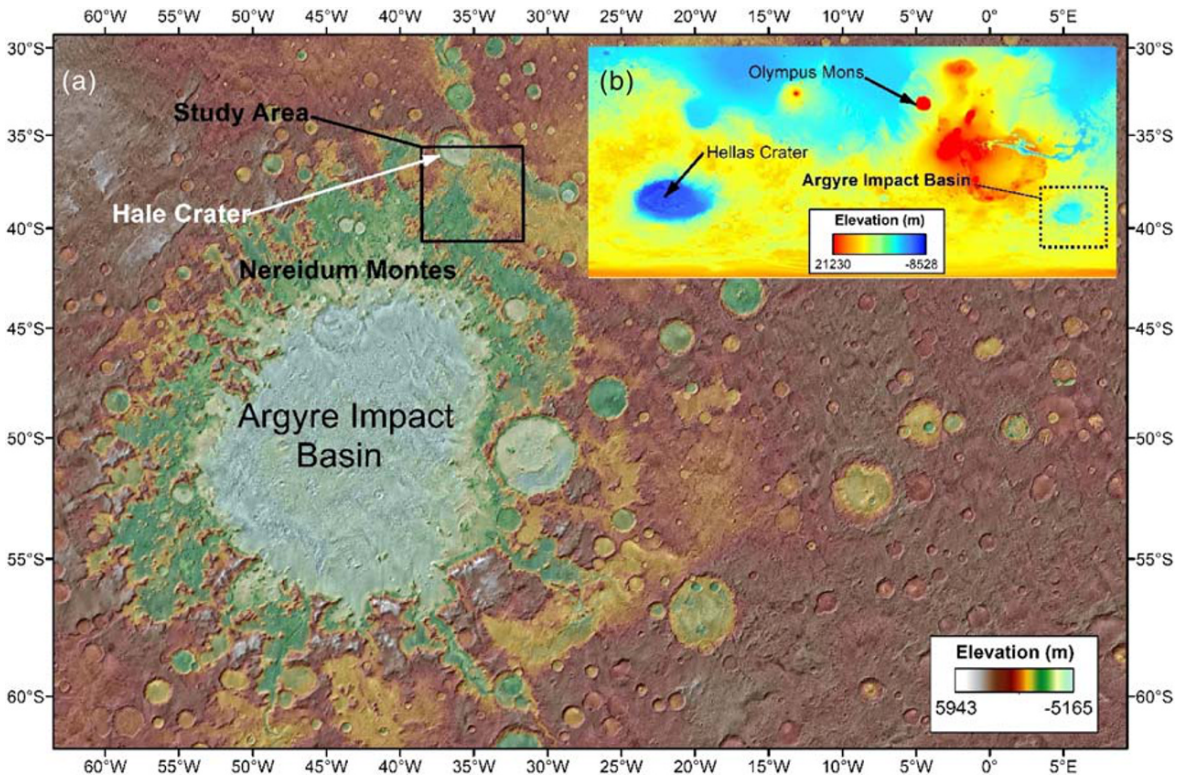

Figure 1. Mars Orbiter Laser Altimeter (MOLA) gridded elevation data overlain with Thermal Emission Imaging System (THEMIS) daytime infrared imagery, highlighting the location of Hale crater within the Argyre Basin. (b) MOLA elevation data overlain with the location of the Argyre Impact Basin in Mars's southern hemisphere. Note: color scales differ between (a) and (b) for ease of visibility. North is upward in all figures.

Subsurface and Ionosphere Sounding (MARSIS) instruments have vertical resolutions that are too low to detect the top of most near surface ice deposits, at 15 m (Seu et al., 2007) and 150 m (Picardi et al., 2005), respectively. Furthermore, the large spatial footprint of gamma ray and neutron data sets shows only regional trends in ice abundance. The ejecta produced by meteorite impacts offers a solution, as they can provide insights into local ground conditions at the time of impact crater formation.

Crater impacts allow access to the subsurface across Mars as they incorporate material from depth into their ejecta (Weiss et al., 2017). By studying ejecta characteristics, the properties of the surface and subsurface (e.g., volatile content) can be inferred. For example, single-layered, double-layered, and multilayered ejecta blankets may indicate the presence of volatiles in the subsurface (Barlow & Perez, 2003). Rampart (Mouginis-Mark, 1987), ring mold (Kress & Head, 2008), and pedestal craters (Kadish et al., 2008) may also indicate impact into ice-rich substrates and then subsequent evolution of the ejecta deposits (i.e., through sublimation). Many individual craters on Mars, such as Lyot (Weiss et al., 2017), Tooting (Morris et al., 2010), and Bakhuysen (Caudill et al., 2018), exhibit channels and polygons interpreted to be suggestive of ejecta material that contained volatiles. However, few in-depth analyses of individual Martian ejecta blankets have been conducted (Caudill et al., 2018).

This study documents landforms in the southern region of Hale crater's (Figure 1a) ejecta and presents a model for their evolution. Hale crater offers an excellent opportunity to analyze ejecta that may have contained volatiles, due to its size and comparatively young age. Hale crater formed in the Amazonian, approximately ~1 Ga ago (Jones et al., 2011). This is 600 million years younger than Lyot crater (Weiss et al., 2017) and over 1 Ga younger than Bakhuysen crater (Caudill et al., 2018). Hale crater is also larger and deeper than almost all craters of its age. Consequently, Hale crater has some of the best-preserved deposits of former subsurface material for a crater of its size and contains smaller scale (~10–20 m) features that have been eroded away in other ejecta blankets. These features can be investigated by in-depth regional studies, which have been conducted for two locations in the Hale crater region: one within the proximal ejecta deposits

(distances within 5 crater radii) filling Moanda crater to the southwest of Hale (El-Maarry et al., 2013) and for Hale crater's distal ejecta deposits (distances greater than 5 crater radii), to the north and northwest of the impact site (Grant & Wilson, 2018). A general geomorphic analysis of the crater cavity and surrounding landscape has been completed, from which the energy released by the impact and the estimated flow volumes for a series of "channels" to the northwest of the crater has been calculated (Jones et al., 2011). However, several areas of Hale crater's ejecta have not been analyzed to this level of detail (El-Maarry et al., 2013; Grant & Wilson, 2018; Jones et al., 2011), including the most extensive and densely clustered landforms thought to be associated with the impact, located immediately south of the crater. This paper maps and characterizes these landforms in detail, synthesizing the results with previous work to produce a model for the emplacement and evolution of these deposits. From these findings we (1) assess the likely geomorphic processes that have led to the current morphology of the ejecta blanket and (2) assess what these landforms suggest about the volatile content of Hale crater's ejecta.

2. Geological and Regional Setting

Hale crater is an ~137 km diameter crater centered at 35.7°S, 323.4°E (Figure 1) (Jones et al., 2011) within the Nereidum Mountain Range, which forms the northern rim of the Argyre Basin in Mars' southern hemisphere (Figures 1b and 1c). The impactor that created Hale crater struck from SE to NW (Schultz & Wrobel, 2012) and hit a region of the Argyre Basin thought to contain a former section of Uzboi Valles (Jones et al., 2011). When it was active during the Late Noachian and Early Hesperian epochs, Uzboi Valles would have transferred 150,000–450,000 $m^3 s^{-1}$ of water between the Argyre Basin and the northern plains of Mars (Grant & Parker, 2002) and potentially saturated the subsurface through transmission losses into the channel bed. Large volumes of subsurface ice could have developed under this scenario by the time of the Hale crater impact in the Amazonian epoch (Jones et al., 2011). Ejecta almost entirely blankets the mountains and upland areas close to the rim of Hale crater, forming areas of continuous coverage. Discontinuous ejecta deposits cover a wide region of Nereidum Montes, and there is localized accumulation of ejecta in many of the valleys and basins of the range. Further afield, secondary crater chains and rays associated with the impact are present (Schultz & Wrobel, 2012).

The study site for this work is approximately ~190,000 km^2 in area and covers an elevation range of over 5,000 m (Figure 1a). It encompasses the continuous ejecta blanket and the transitional boundary to discontinuous ejecta zone south of Hale crater, where the greatest number of channels associated with the impact site have been mapped (Jones et al., 2011). Throughout this paper, we will refer to the features termed "channels" in previous literature (e.g., El-Maarry et al., 2013; Jones et al., 2011) and the features mapped in this work as "linear depressions," as the latter term does not imply a formation mechanism. "Valleys" here refer to two large lower elevation regions that exist within the rugged uplands area of the study region, which we term Hale Crater Valley 1 (HCV 1) and Hale Crater Valley 2 (HCV 2) (Figure 2).

3. Methods

We used a variety of data sources and methods to explore the morphology and formation of the landforms in the study area. Individual Context Camera (CTX; Malin et al., 2007) images at ~6 m resolution were the primary data source used for observations and mapping of the study site. High Resolution Imaging Science Experiment (HiRISE; McEwen et al., 2007) data at 51 cm resolution (2 × 2 binning) were used to the resolve the smallest surface features and textures where coverage allowed, in order to aid interpretation of CTX data. Mars Orbiter Laser Altimeter (MOLA) gridded elevation data (Smith et al., 2001), High Resolution Stereo Camera (HRSC) data (*h0511_0000.da4.53*) (Jaumann et al., 2007), and a HiRISE stereo pair derived digital elevation model (DEM) were used for the extraction of elevation profiles and contours. The HiRISE DEM was produced from HiRISE Images *ESP_013665_1420 and ESP_012808_1420* using the software SOCET SET, following the method outlined by Kirk et al. (2009). A MOLA-HRSC blended DEM was used for the background elevation in context maps but was not used for the analyses. All data were projected into a Lambert Conformal Conic projection with the parallels set at 35°S and 55°S to reduce distortion.

Data sets were imported into ArcGIS software to produce geomorphic maps, elevation profiles, and contours. The locations of the study site maps are shown in Figure 2a. All landforms were mapped using individual CTX tiles due to their consistent coverage across the study area and their higher resolution than

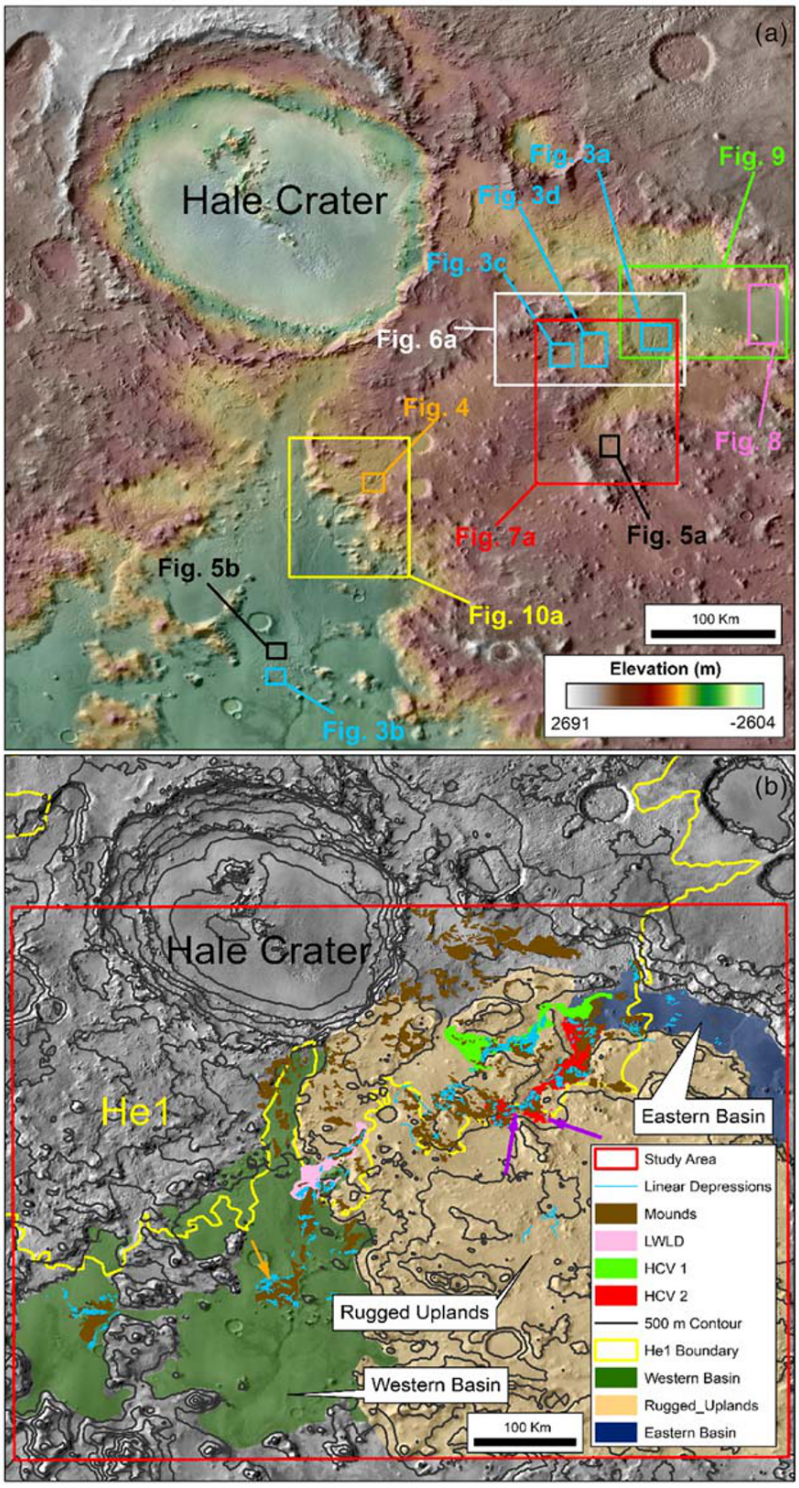

Figure 2. (a) MOLA-HRSC blended elevation data overlain THEMIS daytime infrared imagery, highlighting the topography of the study area, and figure locations. (b) THEMIS infrared imagery overlain by a MOLA-HRSC derived hillshade model and the locations of the linear depressions, ejecta mounds, and polygons. Polygons are not visible at this scale, so are indicated by an orange and purple arrow. The purple arrow indicates the raised rim polygon locations and the orange arrow indicates the high center polygon locations. Also highlighted are Hale Crater Valley 1 (HCV1), Hale Crater Valley 2 (HCV2), the Large Western linear Depression (LWLD), the Eastern Basin, Western Basin, and the Rugged Uplands adjacent to Hale crater. The boundary of the He1 ejecta unit as defined by Jones et al. (2011) is also included. All ejecta outside of this boundary is considered to be the He2 ejecta unit.

blended CTX tiles. Landforms were delineated by the extent of similar surface morphologies at CTX resolution and mapped at a scale of 1:15:000.

4. Results

Three distinct types of landforms associated with the Hale ejecta were mapped: (i) linear depressions that incise the ejecta material, (ii) mounds within the ejecta, and (iii) polygonal surfaces. The linear depression and mounds are principally located upon the Rugged Uplands within HCV 1 and HCV 2 (Figure 2). Outside of the Rugged Uplands, linear depressions and mounds are located within the Eastern and Western Basins, which lie to the east and west of the Rugged Uplands respectively (Figure 2b). Polygonized surfaces are much less extensive than the linear depressions and mounds and are limited to just HCV 2 and the Western Basin.

4.1. Linear Depressions

Linear depressions at the study site are primarily situated in a band ~50 km wide that begins ~100 km SE from the central peak of Hale crater, although some can be found up to ~230 km from the crater center (Figure 3). Further examples of linear depressions in the study area have been mapped previously (e.g., Jones et al., 2011); however, these were not included here, as they were interpreted to be either preexisting features, associated with other craters, associated with other deposits that might not be related to Hale crater, or not clearly identifiable as one continuous feature.

Two general categories of linear depression were identified in the study site based upon their size, setting, and morphology; we refer to these as Type 1 and Type 2 linear depressions throughout the paper:

- *Type 1 linear depressions* (Figures 3a and 3b) are typically straight features, with only slight changes in direction along their length and very rare examples of convergence. They are located at the margins of the ejecta deposits and are only present in a few locations over the study area, for example, the Western Basin and the upper region and terminus of HCV 2. Compared to Type 2 linear depressions, they cover a much smaller portion of the study area, as they are shorter (<1–2.4 km) and sparse. The widest Type 1 linear depression is 350 m across, but most are between 50 and 80 m. MOLA elevation data are not of sufficient spatial resolution to determine their depth.
- *Type 2 linear depressions* (Figures 3c and 3d) are generally longer than Type 1 linear depressions, reaching tens of kilometers in length (5–54 km). Being typically 50–150 m wide, Type 2 linear depressions are comparable in width to Type 1 linear depressions, with the widest being 390 m across. Type 2 linear depressions exhibit more changes in direction than Type 1 features, crisscrossing each other and developing anastomosed sections in rare cases. While Type 2 linear features are observed to crosscut each other, they do not have tributaries and there are few examples where these features merge into a single large feature further downslope.

Both Type 1 and Type 2 linear depressions are located solely upon the ejecta material and are not observed beyond its margins (Figure 3). In addition, no linear depressions dissect the rim or interior of Hale crater (Figure 3). Linear depressions of both types usually have one or both ends within ejecta material containing clusters of mounds (Figure 4b) and rarely have both ends solely within smooth ejecta deposits that lack mounds. Linear depressions occur in clusters, and each cluster is separated from other clusters by ~1–60 km. Clusters of linear depressions are commonly located directly upslope or downslope of other clusters, but this is not true for all clusters. No individual linear depression in HCV 1 or 2 has any depositional features such as fans at either end.

Although HCV 1 and 2 contain the most extensive areas of interconnected linear depressions at the study site, the longest and widest linear depression at the study site is located on the opposite side of the rugged uplands (Figure 2). We term this feature the LWLD. LWLD does not display the same interconnected pattern as the linear depressions located in HCV 1 and 2; instead, it is a single large feature. Outside of these areas, linear depressions are also located within two large basins in the east and the west of the study site, and upon the mountains adjacent to Hale crater (Figure 2).

Type 1 and Type 2 linear depressions are located outside of HCV 1, HCV 2, and the LWLD. They are also present within the rugged uplands adjacent to Hale crater and within the basins in the east and west of

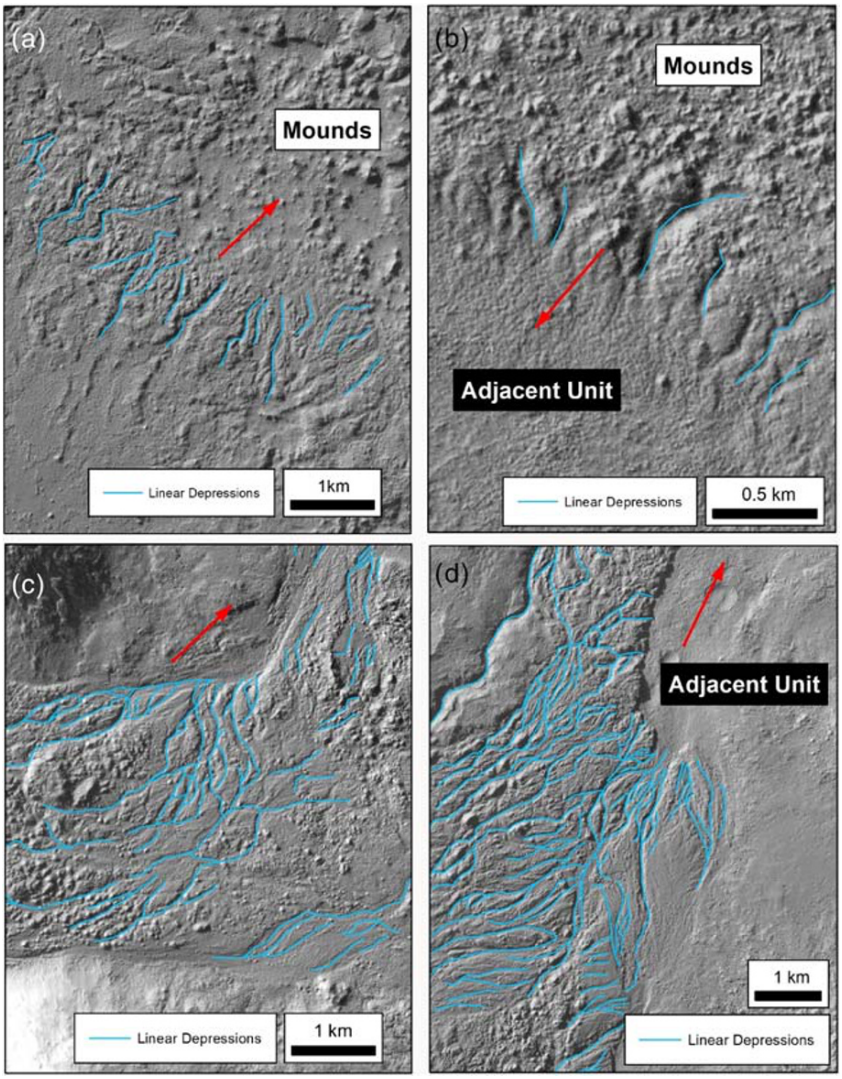

Figure 3. CTX images of Type 1 and Type 2 linear depressions, which are highlighted in blue. The red arrows indicate the downslope direction in all figures. Note: scale in (b) is different to the rest of the figures. (a) Type 1 linear depressions and mounds at the terminus of HCV 2. (b) Showing Type 1 linear depressions and mounds at the margins of an ejecta deposit in the Western Basin. Also visible is a section of ejecta-free surface, labeled as "adjacent unit." (c) Showing Type 2 linear depressions at the head of HCV 1. (d) Type 2 linear depressions in the middle section of HCV 1. Ejecta-free surface is also visible in this location. Image IDs: (a) CTX Image *P19_008628_1431* centered at 36.689°S, 33.537°W, (b) CTX Image *P22_009828_1407* centered at 39.238°S, 36.241°W, (c) CTX Image B01_010118_1433 centered at 36.929°S, 34.149°W, and (d) CTX Image *B01_009907_1433* centered at 36.836°S, 33.883°W.

the study region. These examples are similar to those within the HCVs, though the clusters of linear depressions typically contain fewer and shorter linear depressions than clusters in HCV 1 and HCV 2.

4.2. Mounds

Mound-bearing ejecta deposits are common across the study site (Figure 2b). Clusters of tens to hundreds of mounds are more common than solitary examples (Figure 3). Within these clusters, most mounds are distinct and not interact with other mounds, but on some occasions these landforms do join (Figure 4a). Individual mound morphology varies: The majority of the mounds are slightly elongate (Figures 4a and 4b) or cone shaped (Figures 4c and 4d), but some are tabular. The mounds also vary widely in size, from several tens of meters to half a kilometer in width. Features smaller than 10 m may exist, but these are not clearly distinguishable from boulders at HiRISE resolution. The small size of the mounds compared to the

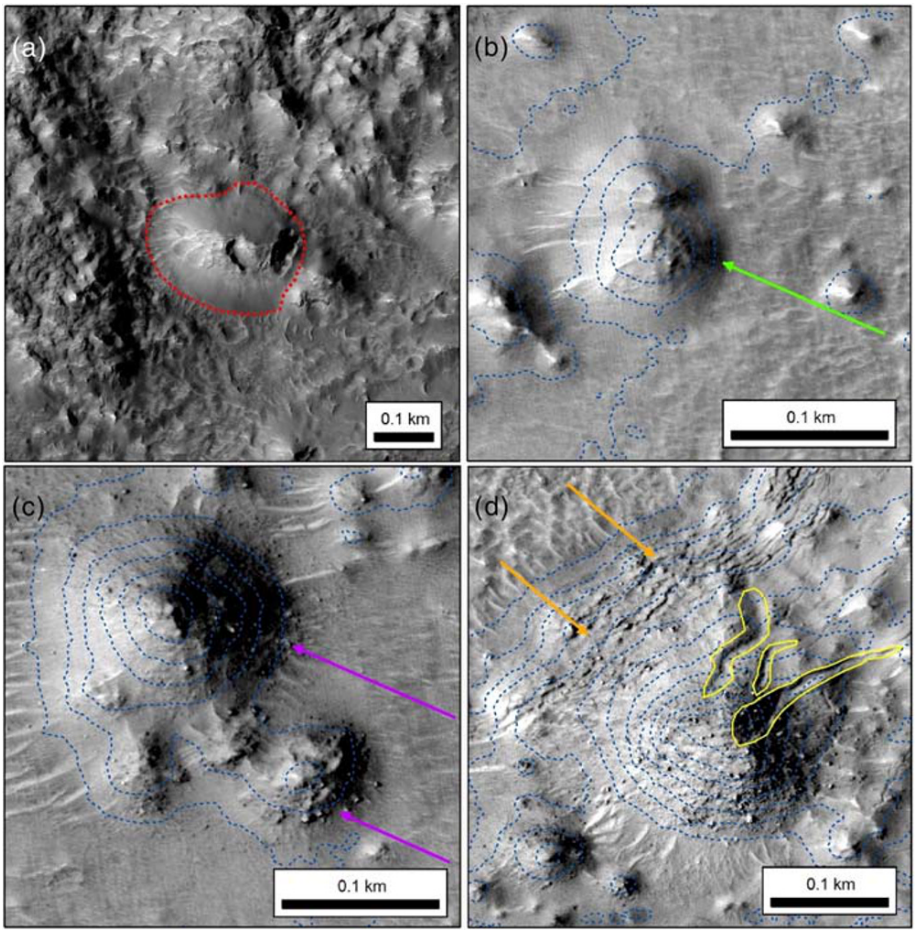

Figure 4. HiRISE images of mounds that exist within the ejecta material. Contours derived from a HiRISE stereo pair (*ESP_013665_1420, ESP_012808_1420*) are at 5 m intervals, aside from Figure 4a, as the DEM does not overlap this region. North is upward in all images. (a) A large mound that has a pit or crater in the summit and the southeastern slope. Surrounding this mound are many other smaller mounds, some of which run up against each other forming an almost complete surface. (b) The region near the head of the LWLD, showing a mound with no block, cracks, or pits on the surface. The green arrow indicates the lack of boulders at the foot of the mound. (c) This figure highlights boulders (indicated by purple arrows) on the summit, sides, and base of two mounds. (d) A mound with crevasses on its surface, as well as tens of boulders. The crevasses on the mound are outlined in yellow. Cracks are also present at a break in slope in the ejecta, and these are marked by orange arrows. Image IDs: (a) HiRISE Image *ESP_029792_1425* centered at 36.644°S, 33.963°W, (b) HiRISE Image *ESP_012808_1420* centered at 37.694°S, 35.388°W, (c) HiRISE Image *ESP_012808_1420* centered at 37.672°S, 35.389°W, and (d) HiRISE Image *ESP_012808_1420* centered at 37.706°S, 35.403°W.

spatial resolution of MOLA and HRSC elevation data, and the lack of suitable HiRISE stereo coverage, prevents detailed analysis of their topography over much of the study area. However, a single HiRISE stereo pair does overlap some of the mounds, allowing elevation profiles to be extracted for 10 examples. The profiles reveal a height range for individual sides of each mound of between 13 and 38 m, with an average height of 29.5 m for the group, and slopes on the mounds' flanks of between 12.9° and 19.6° (average of 16.3°).

The top and sides of some mounds are covered with angular boulders up to 10 m across (Figures 4c and 4d), and these boulders are also visible across much of the ejecta in the study site. We suggest that the boulders are embedded within the mounds and ejecta rather than being selectively deposited on these areas, as there is no obvious possible mechanism to deposit boulders of such size on the surface of the ejecta. Other mounds and regions of ejecta display no boulders on their surface at all (Figures 4a and 4b), but presence of aeolian ridges surrounding some mounds may indicate that boulders in these areas have been buried. Several of the mounds also possess craters or pits on their surfaces (Figure 4a), though others are smooth and unmarked

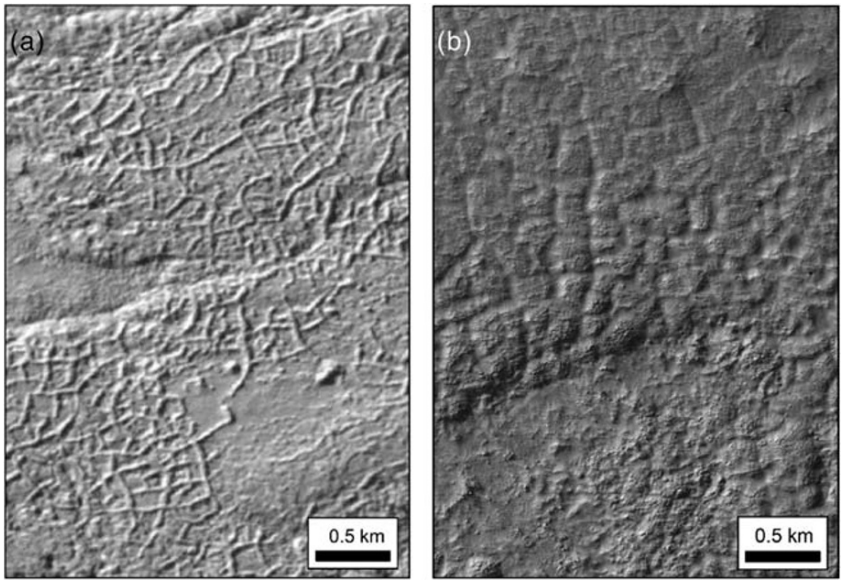

Figure 5. The different polygon types with Hale crater's ejecta material at the study site. Lighting is from the left in both images. (a) Raised rim polygons located in the central part of the study region. (b) High center polygons located in the west of the study site. Image IDs: (a) CTX Image *B01_009907_1433* centered at 36.549°S, 33.774°W and (b) HiRISE Image *ESP_019177_1405* centered at 39.051°S, 36.22°W.

(Figure 4b). Cracks or fractures over 100 m long and tens of meters wide run up the flanks of some larger mounds to the summits (Figure 4d).

Linear depressions frequently have one or both ends among clusters of mounds (Figures 2–4); however, not every cluster of mounds has linear depressions associated with them (Figure 3a). The most extensive regions of mounds lacking any association with linear depressions are found close to Hale crater.

4.3. Polygons

Some regions of the Hale crater ejecta within HCV 2 and in the Western Basin have cracked or ridged surfaces. The interlinking cracks and ridges divide the ejecta surface into polygons, which have raised (Figure 5a) or sunken rims (Figure 5b). Raised and sunken rim polygons are not found near each other. Raised rim polygons are limited to just three areas at the head of HCV 2, at the fringes of ejecta deposits and within a gap separating two clusters of mounds. Raised rim polygons have highly irregular shapes, though some form rough rectangles <100 m long and <70 m wide and occur in patches up to 1.3 km long and 2.3 km wide. Most of the raised rim polygons are completely enclosed on all sides, but those toward the edges of the ejecta material are often not enclosed. Landforms that resemble the rims of the polygons protrude above the ejecta at the fringes of the polygonal surfaces. No linear depressions are associated with this type of polygon.

The sunken rim polygons are primarily located within the Western Basin close to the margins of ejecta flows (Figure 5b) and are rare elsewhere in the study site. They are irregularly shaped and up to 90 m across. Additionally, the rims of these polygons appear to become deeper and more pronounced toward the margins of the ejecta deposits and toward linear depressions.

4.4. Morphology of HCV 1, HCV 2, and the LWLD

The linear depressions, mounds, and polygons in the study area (Figures 2b and 3–5) are most prevalent and well developed in HCV 1, HCV 2, and the LWLD. HCV 1 and HCV 2 are broadly similar in terms of the geomorphological features that they contain and are located close together, separated by a topographic ridge that runs along most of their length. Both valley landform assemblages have their heads within the mountainous terrain adjacent to Hale crater and terminate within the basin in the east of the study site. The distinction between HCV 1 and 2 within the Rugged Uplands and the Eastern Basin was based on the local topography and distribution of linear depressions, which are aligned with one valley or the other. Linear

depressions are common in HCV 1 and 2, incising through smooth ejecta material and through ejecta material that contains mound and block structures. HCV 1 has larger continuous incised ejecta deposits (~150 km^2) than HCV 2 (~50 km^2), which have isolated areas that display surface incisions. The LWLD contains some features similar to HCV 1 and 2 and also some unique features. This section describes landform associations in HCV 1, HCV 2, and the LWLD and compares these regions.

4.4.1. HCV 1

The landforms associated with HCV 1 begin at the head of the valley, located at its southwestern end within the rugged uplands (Figure 6a). Ejecta covers most of the landscape at the head of HCV 1, and clusters of mounds are common (Figure 6b). Type 2 linear depressions commonly have one or both ends within these clusters. In one location, a section of a linear depression is cutoff. The cutoff section of linear depression does not grade down to other linear depression that incises it (Figure 6b) and is instead left hanging above it, a rare occurrence across the study site a whole. Though the linear depressions are aligned to the local elevation gradient, no linear depressions present in the upper valley continue downslope into the middle section of HCV 1, despite the presence of continuous ejecta deposits that reach from the upper valley into its middle section.

The middle section of HCV 1 has clusters of hundreds of mounds (Figure 6c). These mound clusters are associated with many Type 2 linear depressions, most of which are <6 km long and between 130 and 150 m wide, although some are as narrow as 50 m (Figure 6c). One linear depression that runs along the northern margin of the ejecta is an exception (Figures 6c and 6d). It is comparable in width to the other linear depressions but is far longer than the other depressions, at 18.5 km and extends almost the entire length of the middle section. Linear depressions are particularly common around a 5 km wide raised section of ejecta (Figure 6c) and incise the material downslope of it but do not extend beyond the ejecta margins. The number of linear depressions decreases further downslope (Figure 6d) as the ejecta deposit narrows in width toward the Eastern Basin.

The extent of the ejecta surface narrows with distance downslope and HRSC data (*h0511_0000.da4.530*) reveal that the ejecta surface increases downslope by up to 20 m, until it becomes abruptly free of mounds (Figure 6d). Downslope of this location, the surface elevation of the ejecta decreases up to the margin of the continuous ejecta surface, dropping by ~95 m over 2.2 km. This gives the end of the continuous ejecta in the valley a convex-upward profile. Beyond this point, the ejecta surface is discontinuous and mounds are absent (Figure 6d). There are sparse linear depressions, but these are much less distinct than the ones upslope and quickly give way to featureless smooth ejecta deposits. Further downslope, there are no linear depressions similar to those in the middle and upper sections. Here, HCV 1 bifurcates around a raised section of the landscape and converges on its southeastern side then continues as a single valley toward the Eastern Basin (Figure 6a). A 1.1 km wide crater filled with ejecta is present immediately downslope of valley convergence, and it is unclear whether HCV 1 bifurcates around this crater, goes through the center of it, or is possibly routed through all three of these options. Despite this uncertainty, these routes form a clear linkage between the ejecta surfaces within the middle section of HCV 1 and the Eastern Basin and are a possible direct continuation of the linear depressions upslope. However, these linear depressions are up to 1.8 km wide, much larger than the linear depressions upslope, and have craters and scattered ejecta deposits on their floors.

At its terminus, HCV 1 opens out into the Eastern Basin. Here, an extensive region of fractured ejecta spans the exit of the valley (Figure 6d), with more fracturing and larger gaps present in the center. The fractures divide the ejecta into slabs that extend downslope from the north western end of HCV 1 and increase in size further away from the mouth of HCV 1. Gaps between these blocks contain some of the mounds that are present upon the valley floor of HCV 1.

4.4.2. HCV 2

Although both HCV1 and HCV 2 contain many similar landforms, HCV 2 (Figure 7a) is morphologically distinct from HCV 1. One landform that is unique to HCV 2 is the polygonized ejecta surfaces in its upper region (Figure 7b). These polygonal surfaces are located at the fringes of ejecta deposits and can be located within or beyond the ends of linear depressions. The polygonized surfaces in HCV 2 are unique in the study area, as they are the only ones to have polygons with raised rims. A further difference between HCV 1 and HCV 2 is that much larger areas of the valley bottom are devoid of visible features compared to HCV 1 and gaps in the ejecta surface are more common (Figures 7a, 7c, and 7d) particularly on the downslope side of mound clusters. However, ejecta covers the valley sides for the most of their length, even in sections

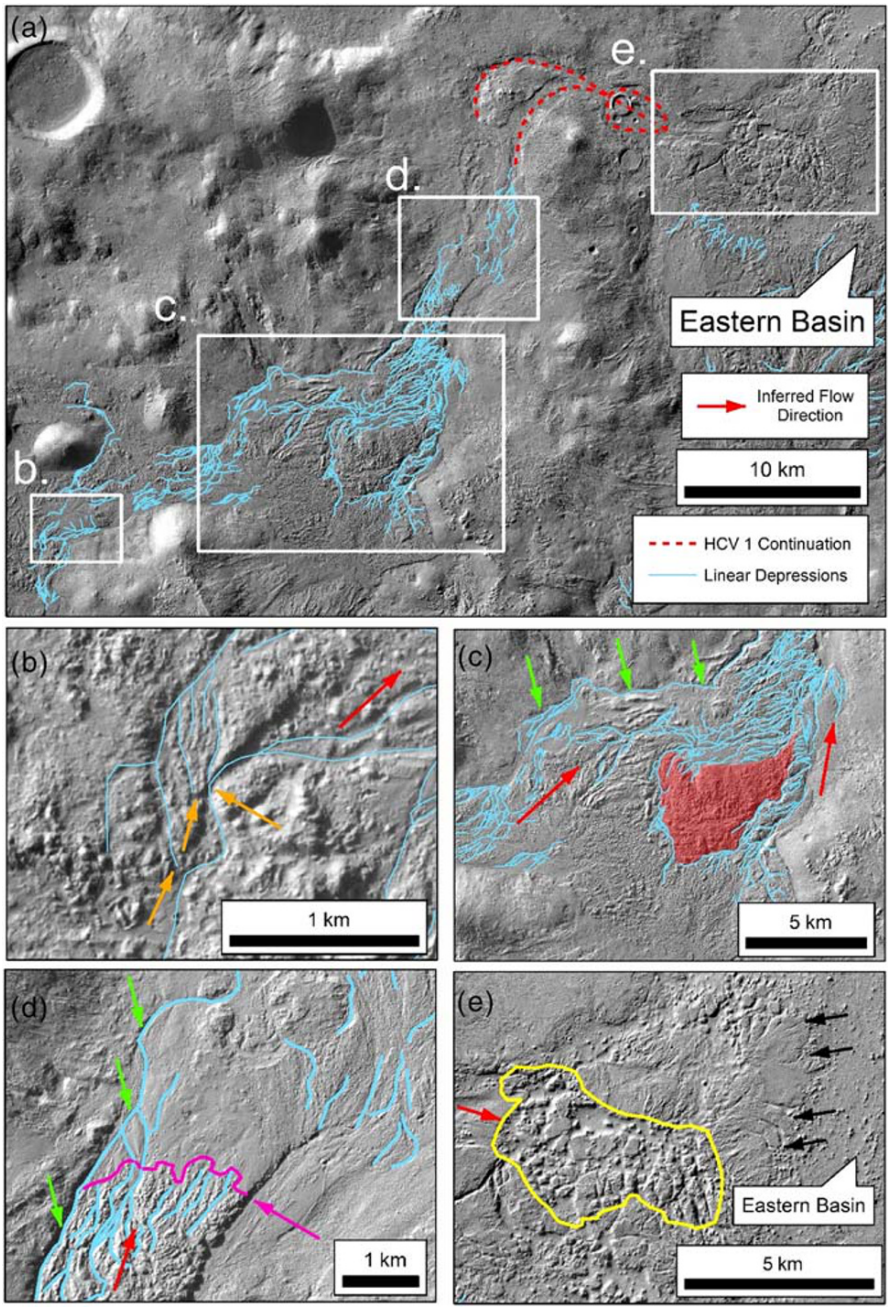

Figure 6. CTX images of landforms within HCV 1. Red arrows indicate inferred flow direction in all images. (a) The locations of linear depressions in HCV 1 and the locations of Figure 6b–6e. The dotted red lines indicate the possible ways that linear depressions may have continued from the edge of the ejecta margin upslope to connect with the Eastern Basin. (b) The upland section of HCV 1. Orange arrows indicates cutoff sections of a linear depression. (c) A region of heavily incised ejecta in the middle of HCV 1. Linear depressions appear to deviate around a large raised section of ejecta, containing tens of mounds, which is highlighted in red. Green arrows indicate an anomalously long linear depression running along the northern margin of the ejecta. (d) The end of the continuous ejecta surface in HCV 1, where the presence of mounds on the ejecta surface ends, and the ejecta transitions to smooth material. This transition is highlighted by a purple line and arrow. Green arrows indicate the continuation of the long linear depression in (c). (e) The splayed ejecta material at the mouth of HCV 1. Black arrows highlight examples of areas where the material has cracked, and the yellow polygon outlines a region of ejecta that has fractured into slabs of material. Image IDs: (a) CTX Images *B01_009907_1433, B01_010118_1433*, and *P19_008628_1431* overlain with MOLA 50 m contours, centered at 36.729°S, 33.952°W; (b) CTX Image *B01_010118_1433* centered at 36.992°S, 34.349°W; (c) CTX Images *B01_009907_1433* and *B01_010118_1433* centered at 36.894°S, 34.014°W; (d) CTX Image *B01_009907_1433* centered at 36.734°S, 33.862°W; and (e) CTX Image *P19_008628_1431* centered at 36.605°S, 34.458°W.

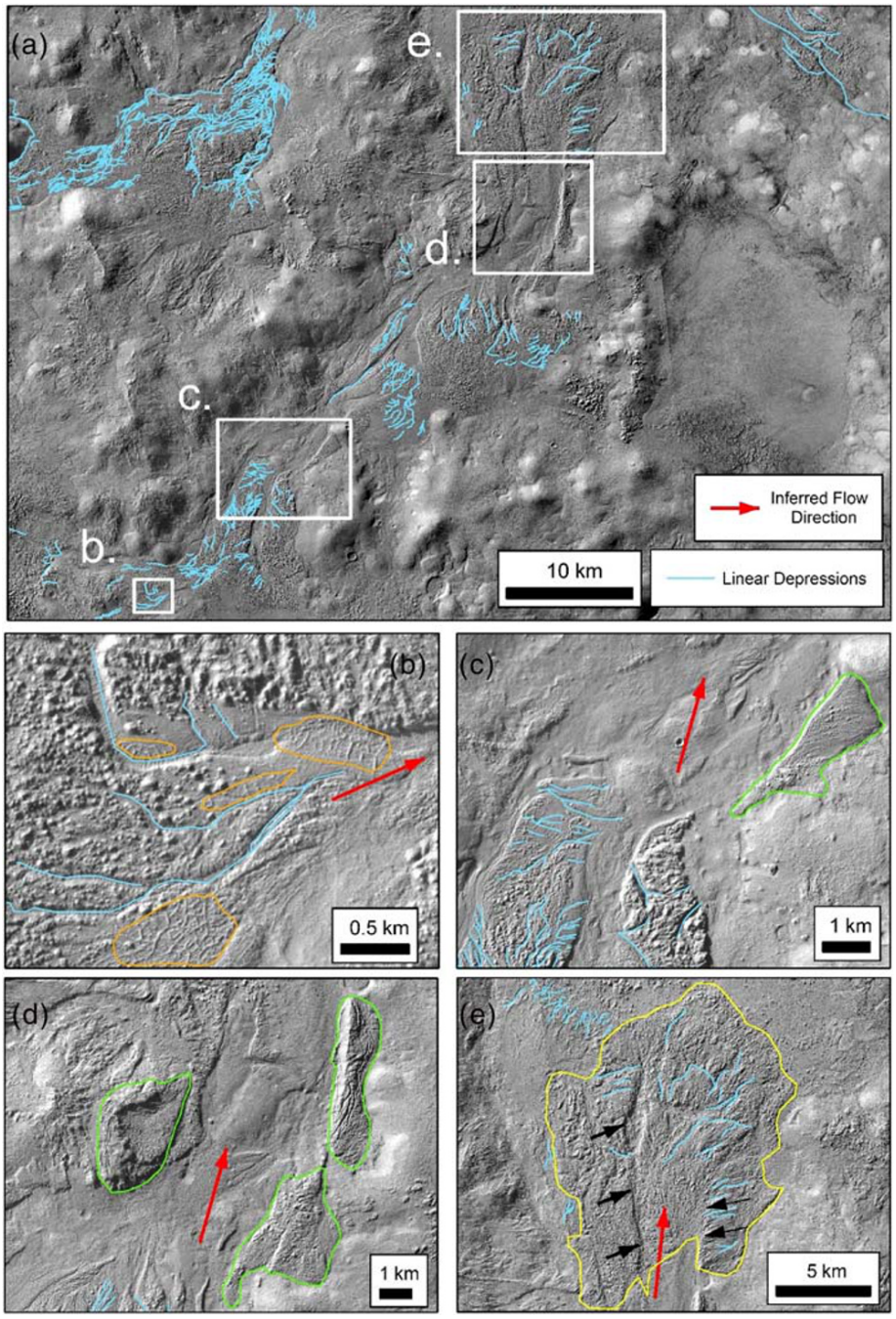

Figure 7. CTX images of landforms within HCV 2. Red arrows indicate inferred flow direction in all images. (a)The outlines of linear depressions within HCV 2 and location of Figures 7b–7e. (b) Linear depressions with raised rim polygons at their bases or in close proximity. Polygonized region are outlined in orange. (c) More examples of incised ejecta and mound clusters. A high-standing, isolated patch of ejecta upon the valley side is outlined in green. (d) Further examples of isolated ejecta deposits, outlined in green, stranded up upon the valley walls. (e) An outline of the fan structure at the mouth of the HCV 2. The fan is outlined in green, and levees in the fans interior are indicated with black arrows. Image IDs: (a) CTX Images *B01_009907_1433*, *G14_023792_1428*, *B01_010118_1433*, and *P19_008628_1431* overlain with MOLA 50 m contours, centered at 37.078°S, 33.631°W; (b) CTX Image *B01_010118_1433* centered at 37.504°S, 34.067°W; (c) CTX Image *B01_009907_1433* centered at 37.320°S, 33.858°W; (d) CTX Images *B01_009907_1433* and *P19_008628_1431* centered at 37.018°S, 33.486°W; and (e) CTX Images *B01_009907_1433* and *P19_008628_1431* centered at 36.809°S, 33.436°W.

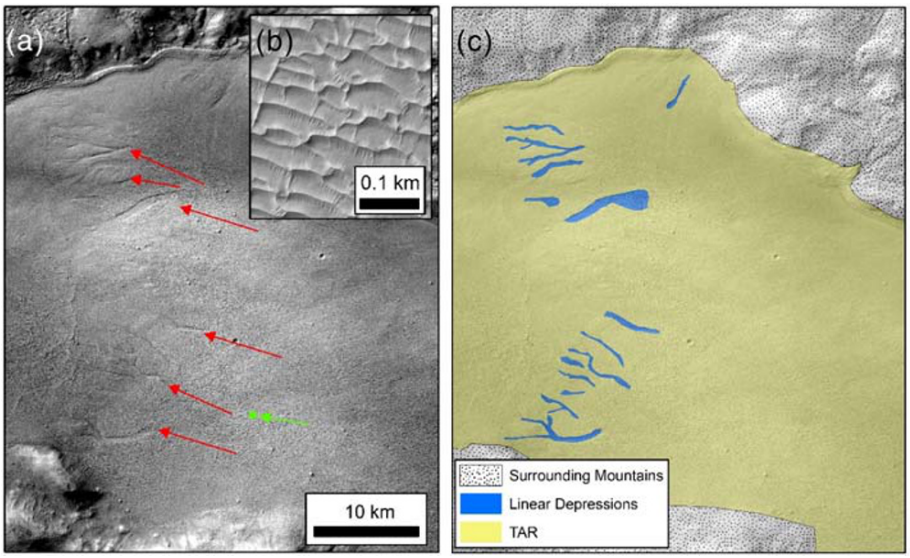

Figure 8. (a) Linear depressions located in the Eastern Basin and the location of (b). These depressions are indicated by red arrows in (a) and are illustrated in (c). The location of (b) is highlighted by a green box and a green arrow. (b) Examples of transverse aeolian ridges that fill the Eastern Basin. (c) An illustration of the linear depressions highlighted in (a). Image ID: (a) CTX Image *G16_024491_1432* centered at 36.594°S, 32.67°W and (b) HiRISE Image *ESP_025137_1430* centered at 36.707°S, 32.543°W.

where the valley floor is bare, and forms high-standing mounds of material rising 100 m from the valley floor. One example is located in the upper section of HCV 2 (indicated by a green polygon in Figure 7c), which has a predominantly smooth surface but rows of mounds in places. Despite these differences, many similarities exist between the upper regions of HCV 1 and HCV 2. The downslope ends of mound clusters comprise smooth material incised by linear depressions, as in HCV 1 (Figure 6d). Additionally, linear depressions originating in the upper valley do not link up with those in the middle section; instead, they reach the edges of the ejecta deposits and vanish beneath them.

Moving downslope, further ejecta deposits with mounds and Type 2 linear depressions occupying the valley floor are found. These landforms span most of the valley floor, with additional isolated and raised patches of ejecta on the valley sides (Figure 7d). There is a sharp boundary between raised ejecta deposits and the adjacent ejecta-free areas of the valley floor. Fracturing is evident on these raised surfaces, with some indications of slumping of the material inward toward the center of HCV 2.

Where HCV 2 opens out into the Eastern Basin, there is a 19 km wide and 20 km long fan-shaped landform with surface mounds (Figure 7e). In the center of the fan is a roughly rectangular 50 m deep depression that shallows relative to the surrounding fan material toward the northern end of the fan. The center of the depression is filled with mounds, though these mounds have wider spacing between them than those elsewhere on the fan landform. Linear depressions of both types incise the margins of the fan and the edges of the central depression.

4.5. Eastern Basin

HCV1 and HCV 2 terminate in the Eastern Basin. Here, a series of linear depressions incise the margin of an ejecta lobe that fills the basin (Figure 8). The linear depressions on this lobe are up to 4.0 km long and 490 m wide, with the smallest 1 km long and 14 m wide. All these linear depressions start and end abruptly, with some evidence of convergence in places. They are most similar to Type 1 linear depressions due to their limited convergence and appearance at the ejecta margin; however, they are much larger than the other Type 1 linear depression at the end of HCV 2 and the Western Basin. They begin at different locations on the lobe, across an east-to-west zone 11 km wide (Figure 9b) across an elevation range of 37 m, resulting in this part of the lobe having an average surface slope of ~0.2°.

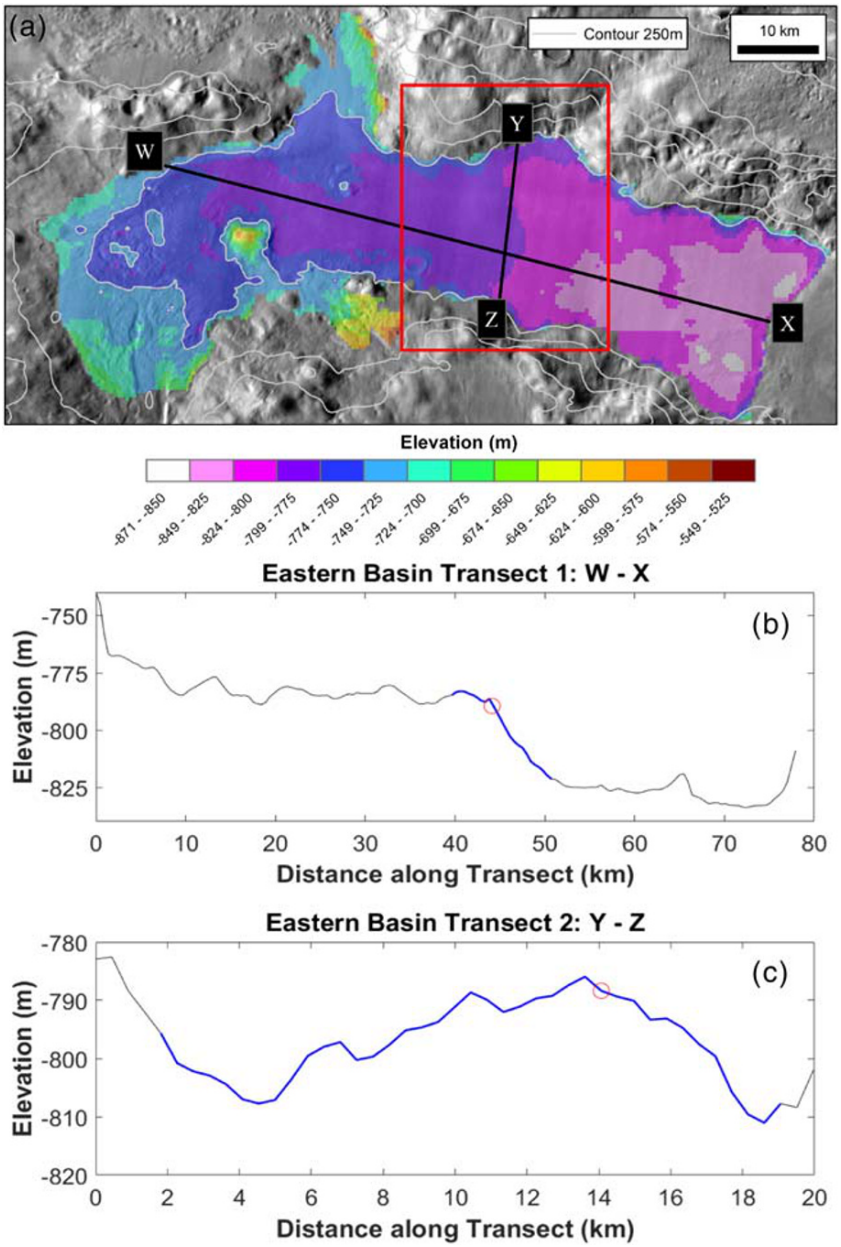

Figure 9. (a) THEMIS imagery overlain with MOLA-HRSC blended elevation data centered at 36.517°S, 32.906°W, clipped to the borders of the basin in the east of the study site. Also shown are the locations of two transects taken from W-X and from Y-Z. The red box highlights the location of Figures 8a and 8b. (b) The elevation profile of Transect W-X in (a). (c) The elevation profile of the Transect Y-Z in (a). The red circles in (b) and (c) show where the transects meet, and the blue sections outline where the zone of linear depressions in Figure 8 are covered by the transect. Elevation transects were extracted from MOLA gridded elevation data.

The lobate appearance of the ejecta in the Eastern Basin is not obvious in visible CTX imagery (Figure 8a). This is because aeolian bedforms such as transverse aeolian ridges (TARs; e.g., Balme et al., 2008) (Figures 8b and 8c) fill the basin and obscure the lobe margins. However, MOLA elevation data show that this lobe comprises a 7.2 km wide deposit that has a convex upward cross profile (Figure 9c) and reaches a maximum height of 45 m relative to the adjacent surfaces.

4.6. LWLD

The longest single linear depression at the study site, the LWLD, runs for 53 km from the mountainous region close to Hale crater into the basin in the west of the study site (Figure 10a). This feature starts at

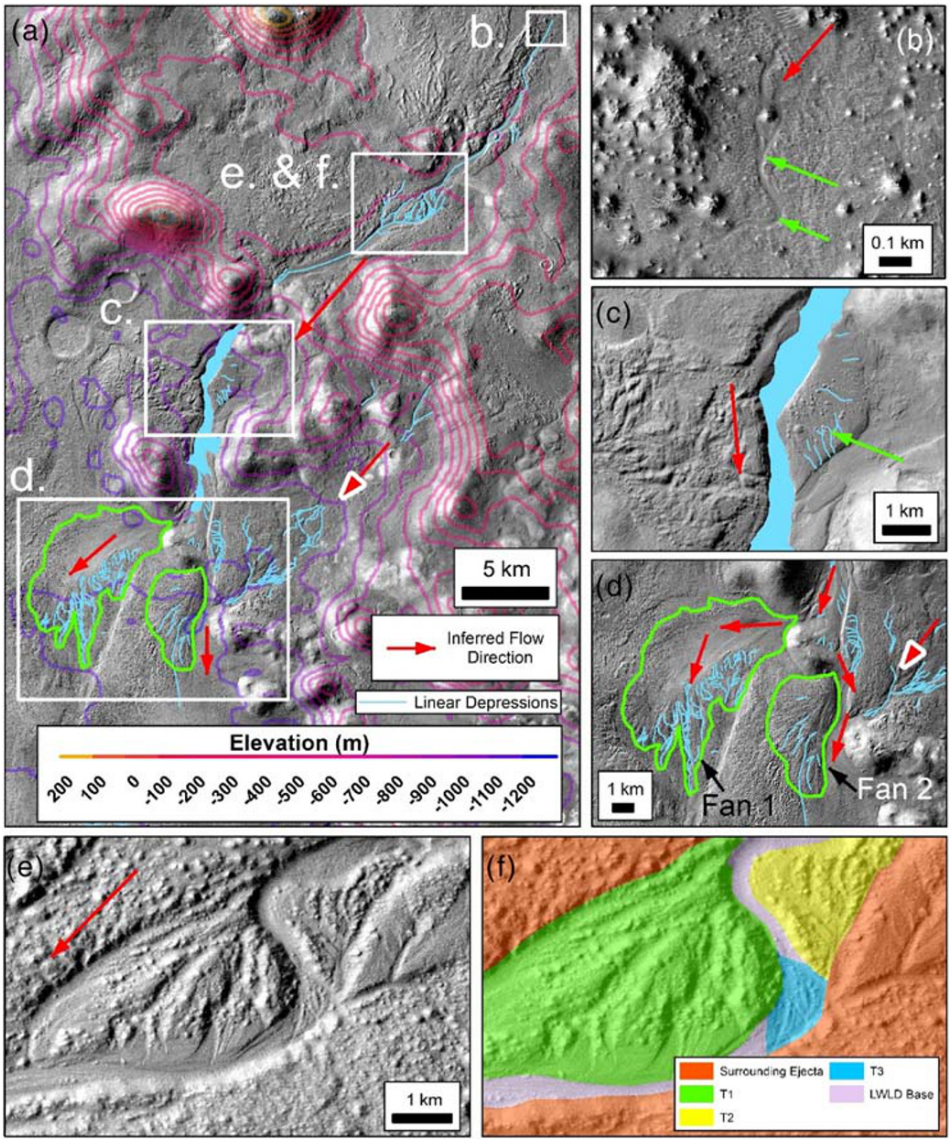

Figure 10. (a) The LWLD and the locations of (b)–(f). Highlighted in green are two fans that are present at the downslope end of the LWLD. (b) The start of the small linear depression that feeds into the head of the LWLD. (c) The middle region of the linear depression. A green arrow highlights a high-standing ejecta deposit, bordering the linear depression. The red arrow with the red and white arrowhead indicates the direction of a second set of linear depressions that feed into the distal region of the LWLD. (d) The terminus of the LWLD. Black arrows indicate the inferred direction of ejecta flow, and green polygons outline the two fans present here. (e) Cutoff linear depressions and terraces. (f) An illustration of the terraces visible in (e). T1, T2, T3 refer to the terrace levels in (f) with T1 being the highest terrace and T3 the lowest. Image IDs: (a) CTX Images *P17_007758_1418*, *P03_002220_1418, B10_013665_1423*, and *G11_022579_1399* overlain with 50 m MOLA derived contours, centered at 38.056°S, 35.699°W; (b) HiRISE Image *ESP_012808_1420* centered at 37.681°S, 35.394°W; (c) CTX Image *P17_007758_1418* centered at 38.038°S, 35.814°W; (d) CTX Image *P17_007758_1418* centered at 38.228°S, 35.89°W; and (e) CTX Image *P17_007758_1418* centered at 37.862°S, 35.552°W.

an elevation of ~ −500 m and terminates at ~ −1,100 m, giving a mean gradient of ~1%. The linear depression is primarily a single depression originating within the ejecta material blanketing the rugged uplands. However, at its head there are several smaller linear depressions 30–48 m wide that feed into the start of the LWLD (Figure 10b). Where these smaller linear depressions enter the LWLD, the depression increases in width to 260 m. Such rapid changes in width are common along the LWLD from north to south, which ranges from 65 m to over 1.6 km wide. The majority of the smaller linear depressions in HCV 1 and 2 do not vary appreciably in width, making the LWLD very different in its along-track width properties.

At 10.5 km downslope from the northern end of the LWLD, sections of blocky ejecta incised by nested and cutoff linear depressions are present (Figures 10c and 10d). Elevation data are not of sufficient spatial resolution to resolve the height differences between these nested linear depressions, but we assume that lower surfaces formed later than upper surfaces. This is very rare in the study site, with the only other example of abandoned/cutoff depressions located in the upper reaches of HCV 1 (Figure 6b). Beyond this section, the LWLD exits the blocky ejecta material and is characterized by large changes in width downslope as it passes between further ejecta deposits (Figure 10e). The ejecta to the east is scattered with some blocky ejecta, is incised by linear depressions and is somewhat similar to the higher-standing deposits located in HCV 2 (Figure 7d). The deposit to the west is heavily fissured and fractured, with no linear depressions.

At the end of the LWLD, the system bifurcates; one part of the LWLD routes west, and the other southward. A separate system of linear depressions joins the terminal region of the LWLD from the north east (white and red tipped arrow, Figure 10d), and both of these systems feed into two fan-like landforms (Figure 10f). The larger fan (Fan 1) splays outward to the west from the western mouth of the LWLD, and the second (Fan 2) is located to the south east, downslope of the separate section of linear depressions. Fan 2 is incised by the southern section of the LWLD, disconnecting it from the linear depressions upslope. The surfaces of both fans are characterized by mounds, like the fan in HCV 2 (Figure 7e).

Linear depressions of both types are associated with both fans, though they emanate from the south western margin of Fan 1 and are located on the fan surface of Fan 2. In both fans, the linear depressions are much shorter and thinner than the LWLD, and are more like those in HCV 1 and 2.

5. Discussion and Analysis

The linear depressions, polygons, and mounds in the study region are located solely in the Hale crater ejecta and within close geographical proximity to the impact site (Figure 2). The landforms we observed in our study area are predominantly associated with the boundary between the He1 and He2 ejecta deposits (Figure 2b), which are two distinct deposits identified in the Hale ejecta blanket (Jones et al., 2011). He1 is defined by Jones et al. (2011) as a proximal ejecta deposit located within Hale crater and upon the landscape immediately surrounding the crater, which has a “rough” appearance. He2 is further from Hale crater than He1 and is composed of discontinuous ejecta deposits that are thinner and smoother than He1 deposits. (Jones et al., 2011). Not all features are located at this boundary, including the linear depressions, mounds, and polygons in the Western Basin (Figure 2b), but they still lie within the ejecta margins. Overall, this distribution strongly suggests that these landforms are the result of processes that occurred within the ejecta blanket as a result of the meteor impact, rather than preexisting landforms that have been buried by ejecta material postimpact, an interpretation consistent with previous work (i.e., El-Maarry et al., 2013; Grant & Wilson, 2018; Jones et al., 2011).

Here we analyze the geomorphology of the mounds, polygons, and linear depressions within the ejecta, as well as the overall appearance of the ejecta, to interpret the processes of their formation. We compare these findings to previous geomorphological analyses of Hale crater's distal deposits (Grant & Wilson, 2018) and the landforms to the southwest of Hale crater that are hypothesized to have also been formed through the Hale impact (El-Maarry et al., 2013). Comparisons are also made to ejecta deposits in other Martian craters. These comparisons aid in determining what may have driven the distribution of landforms across the study site and Hale crater's ejecta. Finally, we outline the implications for the volatile origin and content of the ejecta.

5.1. Linear Depressions

The downslope orientation and sinuous planform of the linear depressions leads us to interpret them as having formed from a surficial fluid, which we infer to have been water due to the lack of evidence for other sources such as lava. This is consistent with other studies of Hale crater ejecta (El-Maarry et al., 2013; Grant & Wilson, 2018; Jones et al., 2011).

The setting and morphology of the linear depressions suggest that the water was released through dewatering of the ejecta material itself. While there is some evidence of hydrothermal alteration of minerals within Hale crater (Dohm et al., 2015), the locations of the linear depressions in the study site indicate that they are not hydrothermally generated, as such systems should be most prevalent within the crater cavity (Abramov

& Kring, 2005). A direct meteorite impact into a surface ice layer would result in sufficient melting to generate networks like those at Hale. This process has been suggested as the formation mechanism for channel networks at Hale crater (Jones et al., 2011) and other craters, such as Sinton Crater (Morgan & Head, 2009). However, such melting should be greatest closest to the rim where the ejecta would have been thickest and hottest, which is not the case at Hale crater (Figure 2b). The linear depressions are instead most prominent where the ejecta has flowed through constrictions in the landscape and at the termini of the ejecta margins. Additionally, unlike Sinton crater (Morgan & Head, 2009) the heads of the linear depressions within the Hale ejecta clearly start within the ejecta material (Figures 3a, 3b, 6a, and 10b). Finally, estimations of the flow volumes within "channels" to the north west of Hale crater, which are the same type of feature as the linear depressions mapped in this study, suggest that a surface ice layer would provide insufficient water to carve these features (Jones et al., 2011).

Rainfall onto the ejecta has been proposed as a formation mechanism for incised networks surrounding other impact craters on Mars such as Mojave and Reuyl (Goddard et al., 2014; Vijayan et al., 2020). The Mojave impact site is a particularly good comparison to Hale crater, as both Hale and Mojave crater are located within outflow channels theorized to be a major water conduits in the past, so similar mechanisms for forming these linear depressions are considered. The rainfall at Mojave crater occurred following (i) the collapse of an impact plume or (ii) volatile release from impact melt (Goddard et al., 2014).

We argue that the impact plume causing rainfall at Hale is unlikely, as Hale crater was formed from an oblique impact striking from SE-NW (Schultz & Wrobel, 2012). Consequently, the plume and associated rainfall should have been strongest in this direction (Goddard et al., 2014), and yet the greatest density of linear depressions is located to the south of the crater.

Precipitation following volatile release from impact melt is also unlikely to have formed the linear depressions in our study areas. At Mojave crater, pitted impact melt material in the crater's interior is theorized to have released volatiles into the atmosphere, which then fell back as rainfall and created channels that emanate from elevated regions of topography. Similar pitted materials are present close to Hale crater's rim and in its interior (Jones et al., 2011), raising the possibility that the linear depressions mapped in this work also formed as a result of rainfall. However, rainfall associated with impact melt should be most intense close to the pitted melt materials, but unlike at Mojave crater, there is no overlap between these pitted materials and the linear depressions at the study site. Additionally, precipitation tends to produce fairly uniform distributions of channels in the areas that it occurs within and should have incised other surfaces, not just the ejecta (Williams & Malin, 2008). This is not the case in the study site, where linear depressions are clustered together, and though there is evidence that water has flowed out from the ejecta over other surfaces (Figure 6a), there are no examples of where water has eroded them. This distribution also likely rules out snowmelt providing the necessary water, as this would also be expected to occur over much wider areas than the clusters of linear depressions at the study site cover (Goddard et al., 2014).

Another difference between the Hale crater linear depressions and those at Mojave is that many of the incised surfaces in the study region are located upon valley floors such as in HCV 1 and HCV 2, and the linear depressions begin within the ejecta in these areas. The majority of channels associated with Mojave crater are sourced from ridge crests (Goddard et al., 2014). There is also no development of higher-order stream networks or linear depressions within the crater itself, both of which should be apparent if rainfall occurred as a result of the impact (Goddard et al., 2014; Jones et al., 2011). Pluvial channels also tend to increase in width downslope, which is not the case with the Hale linear depressions. Instead, with the exception of the LWLD, the individual linear depressions remain the same width end to end (Figure 3c, 3d, and 10c). Finally, unlike Mojave, no alluvial fans were associated with any of the linear depressions. Altogether, these differences indicate different formation mechanisms for the Hale linear depressions and Mojave channels (Goddard et al., 2014; Jones et al., 2011; Williams & Malin, 2008) and suggest that they are not the result of precipitation. Therefore, the most likely possibility is that dewatering of the ejecta itself has produced the linear depressions.

5.1.1. Dewatering of the Ejecta

Water can only be released from ejecta material by dewatering when all pore spaces within the ejecta are filled, as any excess water will not be able to remain within the deposit (Jones et al., 2011). Pore spaces are closed as the ejecta material undergoes compaction through compressional forces created by

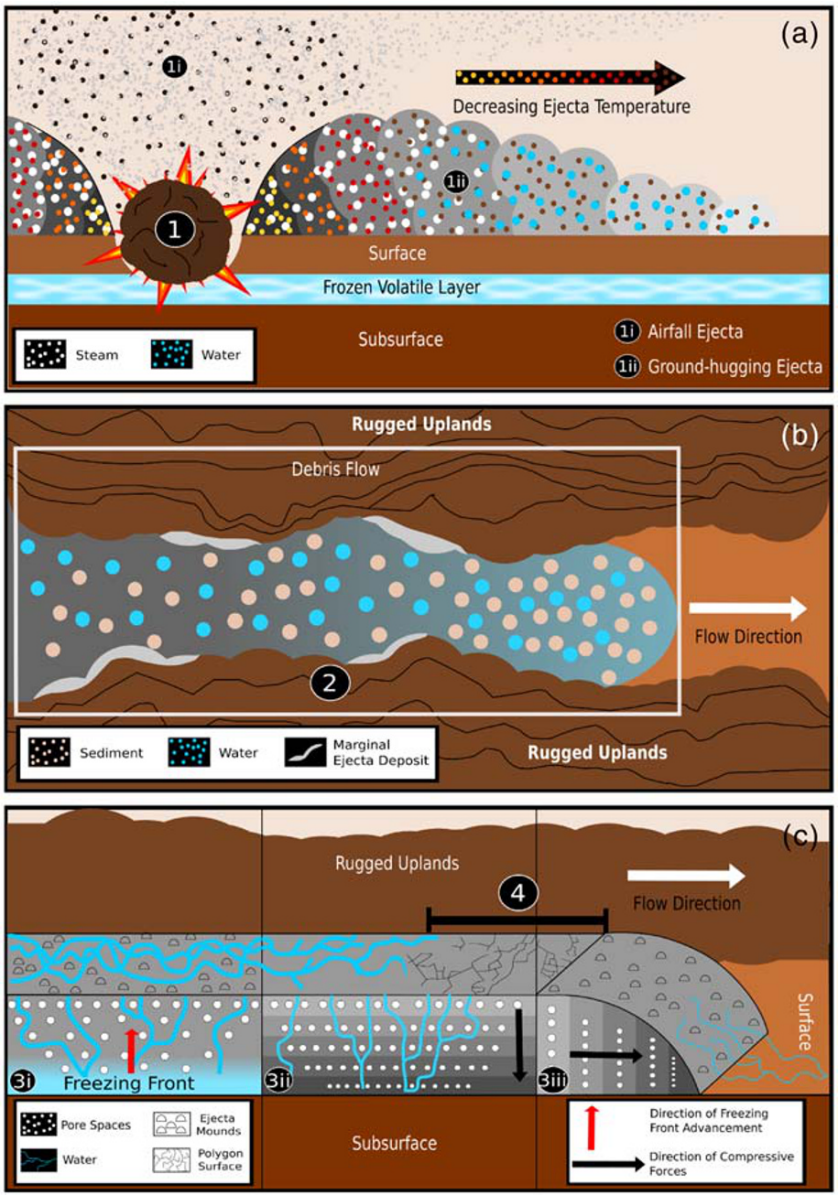

Figure 11. Schematic highlighting the major processes inferred to have occurred during the creation, deposition, and evolution of the Hale ejecta blanket. (a) Cross section of the initial impact and cooling of the ejecta blanket. 1i and 1ii refer to the two different types of ejecta produced in the impact. (b) Plan view of the downslope movement of the ejecta and the formation of the lateral deposits. (c) Three-dimensional view of the proposed mechanisms of ejecta deposit dewatering. The blue lines indicate water-filled linear depressions. Polygonized surfaces are also marked on the deposit surface.

additional flowing material, settling, and possibly freezing (Whelley et al., 2012) (Figure 11c, Points 3i, 3ii, and 3iii). The compaction of deposits is greatest at the base, as this is where load stresses are greatest, so stresses propagate upward over time (Whelley et al., 2012). As pore spaces are squeezed shut, more water is present than can be contained in the available pore space at depth, forcing water to the ejecta surface. Channel incision begins when there is sufficient water flowing on the surface to entrain sediment and incise into the ejecta (Grant & Parker, 2002). We suggest that through this mechanism, the Type 2 linear depressions were created. While Type 1 linear depressions may have also formed this way through very localized overland flow, it is also possible that they formed through sapping, which produces valleys on Earth that are typically shorter and stubbier than features produced by overland flow (Craddock &

Howard, 2002). These sapping features could have formed at the ejecta margins as the margins likely also had increased pore pressures resulting from compaction of material behind the slower moving flow fronts. The unconsolidated and saturated material at the margins would have collapsed in places, and these collapses would have created low-pressure zones that drew in additional water (Major & Iverson, 1999), accelerating the erosion backward from the margins and possibly producing the Type 1 linear depressions. Unlike with the Type 2 linear depressions, the water in this scenario did not flow at the ejecta surface and so did not follow the ejecta surface topography, resulting in limited crosscutting and dissection between linear depressions, something also observed in terrestrial sapping valleys (Craddock & Howard, 2002). However, Type 1 linear depressions are not wider than Type 2 linear depressions, which may be expected if they were formed through sapping as opposed to overland flow.

The lack of obvious alteration in the linear depressions indicates that they must postdate significant ejecta movement. Observed terraces and crosscutting (Figures 6b, 10c, and 10d) could have formed after the ejecta material came to rest and the fluid within the deposit drained away (Crandell, 1971). The paucity of these terraces and cutoff linear depressions elsewhere in the study site suggests that no ejecta movement occurred at the study site after incision of the linear depression networks began, or that it was in very limited locations. It is likely that nearly all linear depression associated with Hale crater postdate significant ejecta movement, as no significant alteration was noted in the linear depressions to the southwest of Hale crater in the Moanda crater valley system (El-Maarry et al., 2013) or in the distal deposits of Hale crater (Grant & Wilson, 2018).

5.1.2. Evidence for Multiple Episodes of Dewatering

Formation of the linear depressions may have been episodic. The different interpreted formation processes of Type 1 and Type 2 linear depressions, and the fact that the LWLD bisects, and thus postdates, Fan 2 (Figures 10a and 10d) supports this. As there are no overlapping ejecta anywhere along HCV 1 and HCV 2, it is not possible to directly determine if the formation of the linear depressions was concurrent between the two valleys. However, a rough estimation of this activity might be inferred from their terminal deposits, which have differing morphologies (Figures 6e and 7e); HCV 1 terminates in a region of splayed and fractured ejecta, whereas HCV 2 terminates in a fan structure. Both of these features are inferred to have formed as material from upslope in HCV 1 and HCV 2 reached the Eastern Basin, as they both splay outward from the mouths of their respective valleys. We infer that the fluid from upslope in HCV 1 must have arrived after sufficient time had passed for the ejecta at the terminus of HCV 1 to consolidate, permitting it to fracture rather than deform. As there are no overlapping or diverted lobes of ejecta in the terminal regions of HCV 1, it is suggested that only one heavily sediment laden flow occurred in this valley, unlike at other craters such has Tooting (Morris et al., 2010), where several sediment laden flows interacted with each other. In HCV 1 the absence of overlapping lobes suggests the fracturing was driven by watery and sediment-poor flows, derived from the dewatering of the upslope ejecta deposits. The lack of fracturing and rafting in the distal region of HCV 2 could suggest that the activity that formed the fan may have been part of the initial surge of ejecta down HCV 2 or from dewatering that occurred soon after the initial surge when the sediment could still deform. This could indicate that dewatering of the ejecta deposits to form the linear depressions in HCV 1 occurred later than in HCV 2.

It is not possible to say exactly how long liquid water was actively shaping the study site from the linear depressions alone. However, there is some evidence for multiple episodes of dewatering. The lack of any incision into the surface units beyond the ejecta margins (Figures 3b and 3d) indicates that water released from the ejecta lacked sufficient duration or power to incise into materials harder than the ejecta blanket. The absence of evidence for the evolution of the flow network into a more efficient and mature drainage system, as seen at other craters such as Sinton (Morgan & Head, 2009), also suggests that the release of water was a time limited event. Consequently, the water was of limited biological use due to the restricted time period it existed in liquid form. This makes the ejecta a much less promising environment in which to find life in comparison to the hydrothermal systems that are theorized to develop in the wake of other crater impacts (Abramov & Kring, 2004, 2005; Turner et al., 2016).

5.1.3. Influence of Topography

The restricted locations of linear depressions within the ejecta at the study site (Figure 2b) suggest that special conditions must have been present in these areas and that ejecta freezing and deflation alone were insufficient to drive the development of linear depressions. Regions with linear depressions may have been

covered by ejecta that contained unusually high amounts of volatiles if these volatiles were not uniformly distributed in the subsurface prior to impact, or the ejecta was not well mixed during transport to these locations. In this scenario, only these areas could produce enough liquid water to fill the pore spaces and result in the dewatering of the deposits. Alternatively, it could be that only these regions generated enough compaction forces to close significant amounts of pore spaces, leading to water being forced from the ejecta material. We suggest that the second possibility is more likely, as linear depressions are better developed where the ejecta material is confined by topography in HCV 1, 2, and the LWLD. A similar geographic distribution was noted in the distal deposits of Hale crater, with linear depressions being located on the ejecta surface in areas where it flowed through topographic constrictions (Grant & Wilson, 2018). However, this is not true for all linear depressions. Type 1 linear depressions are located far from any topographic constrictions, at the terminus of HCV 2 and in the Western Basin. Morphologically similar landforms are also present in the Eastern Basin. This distribution likely reflects a different formation process for Type 1 linear depressions compared to Type 2 linear depressions, reinforcing the suggestion that they are not the result of overland flow. Sapping at the ejecta margins may not be so dependent on topographic constrictions to raise pore pressures, as this extra pressure can be supplied by the compaction of material at the flow margins. Given the typically shorter lengths of Type 1 linear depressions, this process is clearly less effective at extending the length of linear depressions than the process forming Type 2 linear depressions. The longer linear depressions in the Eastern Basin may be the result of greater ejecta thickness there than in the Western Basin and HCV 2. The ejecta in the Easter Basin was confined within the basin and therefore generated greater compaction forces and associated dewatering. High surface slopes do not appear to be a requirement for the production of any type of linear depressions, as the average surface slope of the LWLD and the lobe in the Eastern Basin where they occur is very low, at less than 1° (Figure 9b).

The apparent influence of topographic constrictions, the poorly constrained composition of the ejecta, and a lack of modeling of ejecta dewatering mean that attempts to quantify the volatile content of the entire ejecta blanket by estimating flow in the linear depressions (i.e., through Manning and Darcy-Weisbach equations) will likely result in flow discharge estimates that differ by orders of magnitude (Jaumann et al., 2015). This is because estimations of flow velocity utilizing the Manning and Darcy-Weisbach equations depend on the channel dimensions, flow velocity, and bed roughness chosen for the equations (Jaumann et al., 2015), and none of these factors are tightly constrained for the linear depressions. The exact composition of the ejecta is unknown and likely spatially variable, so bed roughness is would be extremely difficult to determine. Dewatering and outgassing would be occurring all along the length of the linear depressions, which would affect the velocity and friction at the streambed. Even if these factors could be constrained at any given point, some linear depressions such as the LWLD rapidly change in width along their length (i.e., Figure 10), whereas others do not, so estimations of flow would be very dependent on which linear depressions are used and where the profiles are drawn. Finally, it is clear that ejecta material is much less competent than the unit beyond the ejecta (Figures 3, 7c, and 7d), and terrestrial channels are rarely filled to bank-full conditions (Wilson et al., 2004). As a result, these linear depressions are not representative of the flows that occurred within them, even at peak discharge (Jaumann et al., 2015; Wilson et al., 2004). More modeling of the dewatering process is required to make these calculations more accurate.

5.2. Formation of Mounds

The nature and formation mechanism of the mounds within the Hale ejecta (Figures 2, 3, 4, 6, 7, and 10) is unclear. We propose three possible formation mechanisms for the mounds:

A. The mounds are blocks of the crust that were ripped from the surface/subsurface by the impact. These were then incorporated into the ejecta blanket and deposited upon the landscape, before being entrained by flowing ejecta and transported across the surface.
B. The mounds developed as the ejecta spread out after deposition. The ejecta fractured into blocks as it cooled and contracted, and these blocks of ejecta material then degraded over time, giving smoothed sides and a cone shaped appearance (Crandell, 1971).
C. The mounds developed due to differential fluid flow within the ejecta as it flowed across the surface and was deposited (MacPhail, 1973). More liquefied sections of the flow drained around the less liquefied parts of the flowing ejecta, leaving these less liquefied parts as higher-standing mounds (Crandell, 1971).

The roughly consistent and sometimes increasing mound sizes further from Hale crater along the lengths of both HCV 1 and HCV 2 suggests that transport of excavated ejecta blocks across the landscape (Process A) has not produced these mounds. If this were the case, then the mound sizes would be expected to decrease along HCV 1 and 2, as the mounds would degrade more through transportation by ejecta flows (Siebert, 1984). We did not undertake measurements of the geometry of each mound, and the actual flow mechanics and transport distances of the mounds across the study site are unknown, so it is possible that formation of the mounds via ejecta transport may have occurred. However, it is unlikely that the mounds were formed directly due to the impact, as the clustering of mounds in specific areas (Figure 2) indicates association with processes located in these regions and not a widespread random distribution of material with the rest of the ejecta.

We find that the splaying and fracturing of ejecta generating these mounds (Process B) is plausible but unlikely. Several regions of the ejecta have undergone fracturing, (Figures 4d, 5b, and 6e), with the most obvious being the terminal region of HCV 1, which contains splayed sections of ejecta with mounds between them in places (Figure 6e). These mounds could reflect the degradation of previous larger sections of ejecta. However, areas where Hale's ejecta has clearly fractured possess fewer mounds than other regions. One example of this is the terminal region of HCV 1, which contains fewer mounds compared to the valleys of HCV 1 and HCV 2 (Figure 2), even though fracturing is obvious in this region. Additionally, many of the linear depression in HCV 1 and 2 deviate around the mounds, something that is unlikely if the mounds formed from former large sections of ejecta, as the linear depressions should have been routed around the spaces the blocks used to occupy before they degraded. However, Process B cannot be entirely ruled out as multiple processes may have formed the mounds. So the mounds between the fractured slabs at the termini of HCV 1 (Figure 6e) may be different to those in the valleys of HCV 1 (Figure 6d) and HCV 2 (Figure 7b).

While the processes listed above are possible based upon the morphology of the mounds, we find that the most likely explanation for the mounds is that they were formed as the ejecta moved across the landscape (Process C), in a similar manner to how mounds in volcanic avalanches and debris flows form (Crandell, 1971). In this scenario, coarser components such as boulders (Figures 4c and 4d) present within the flows separated from the finer components of the flow through particle segregation and kinetic sieving (Johnson et al., 2012). These coarser components become prominent above the surface either as they rose to the surface through kinetic sieving or as more liquidated and finer ejecta materials flowed around them. The coarsest fractions of mass flows on Earth are able to dissipate pore fluids more easily than the sections composed of finer components (Iverson, 1997), potentially explaining why the most extensive and well-developed mound clusters are located in close association with the linear depressions (Figure 2b), as water could be most easily released from the ejecta in these areas. However, not all mounds are associated with linear depressions. The regions of the study site that have mounds and no linear depressions may have undergone enough movement to create the mounds but not had enough constriction by topography to result in dewatering. Alternatively, they may be the result of Process A or B.

Similar mounds are found in the Moanda crater valley system. The Moanda mounds are 200–250 m across and 30–40 m high, exhibit fractures on their summits, and have comparable average surface slope angles of 17.5° (El-Maarry et al., 2013). However, there are fewer mounds in the Moanda crater valley system than within our study site, and they tend to be isolated (El-Maarry et al., 2013). In the distal deposits of Hale crater, none of these mounds are found. The lack of mounds in these deposits may indicate that the ejecta was more liquefied closer to the crater and more easily able to drain around the mounds or that the boulders in the ejecta material were more difficult or impossible transport to greater distances. The mounds are also not noted in the ejecta of other craters on Mars that have undergone dewatering or produced ejecta flows, and this may signify that the mounds within the Hale ejecta are unique and possibly reflect that the properties of the former subsurface of the impact site were very rare on Mars. Hale crater's location close to Uzboi Valles may indicate that these rare subsurface conditions may have been anomalously high volatile content, but other craters on Mars such as Mojave crater (Goddard et al., 2014) are also located in outflow channels similar to Uzboi Valles, and their ejecta lacks these mounds. Additionally, many other craters hypothesized to have formed in regions with subsurface volatiles, such as those with double layered ejecta blankets, lack similar mounds within their ejecta (Weiss & Head, 2013). It is possible that mounds like these require the

impact to have been of a certain size and that they are still visible at Hale crater due to its relatively young age, whereas they have eroded away at older sites.

5.3. Polygons

Like the mounds, the exact formation mechanism of the polygons is unclear. We do not believe that the polygons are fractures like those at the ejecta flow fronts in the ejecta deposits at Moanda crater (El-Maarry et al., 2013), in the distal ejecta deposits (Grant & Wilson, 2018), or elsewhere in the Hale ejecta (Figures 4d and 7d). The fractures in these areas are perpendicular to the inferred direction of flow and do not form the semiregular network the polygons do. Although other examples of polygonal surfaces similar to the Hale polygons are present elsewhere within the Argyre Basin, (Levy et al., 2009; Soare et al., 2014), we argue that the polygons are related to the Hale impact and not a wider process affecting wider areas of the Argyre basin. The other polygons within Argyre are located within the latitude dependent mantle (Levy et al., 2009; Soare et al., 2014), which the ones at the study site are not, and similar polygons are found within the ejecta surrounding other impact craters, indicating that polygons are a landforms that can be associated with impacts.

Polygons similar and size and morphology to the raised rim Hale polygons (Figure 5a) are located in the ejecta blanket of Lyot Crater (Brooker et al., 2018). While the presence of raised rim or high center polygons is not diagnostic of volatiles, particularly liquid volatiles, (Soare et al., 2014), the Lyot polygons are theorized to indicate the presence of volatiles excavated from depth and incorporated into the ejecta. The Lyot polygons are interpreted to have formed through thermal contraction cracks infilling with windblown material, which then became more resistant to erosion than the surrounding ejecta and left standing above the surface as the material around them degraded (Brooker et al., 2018). No HiRISE imagery of the raised rim Hale polygon features is available, so the same detailed morphometric analysis undertaken at Lyot cannot be attempted here. Even with much more data, such as elevation data or HiRISE resolution images, it would be difficult to determine exactly what type of polygons these are and how they formed (Brooker et al., 2018). However, we consider the same crack-filling process to be a possible formation mechanism for the raised rim Hale polygons, based upon the similar morphology to the Lyot polygons. The raised center polygons may be the same features, without the rims filled in. If the Hale polygons formed in this manner, they may then reflect locally higher concentrations of volatiles in the ejecta, allowing them to form in these small areas and nowhere else. If they did not require volatiles to form, then they indicate another spatially restricted process occurred.

In either case, it is clear that both types the polygons must have formed once the movement of ejecta ceased, or else they would have been destroyed or at least deformed. Raised rim polygons present in the base of linear depressions in HCV 2 (Figure 7b) indicates that they developed after all flows of water and ejecta had ceased, as any further release of water would have incised them and continued ejecta movement would have misshaped them. The raised center polygons must also have formed after the ejecta margin ceased moving, or else they too would have been destroyed.

Overall, the presence of the polygons at the study site may support the former or current presence of volatiles within the ejecta, likely representing the last stage of ejecta evolution and indicate that additional spatial variation in landform development occurred.

5.4. Overall Synthesis

From the landforms we have documented at the study site, we infer a sequence for their formation and implications for the wider ejecta blanket. Initially, as the ejecta blanket was created, volatiles present in the subsurface would have been incorporated into the ejecta and were then carried within it to be deposited in the landscape surrounding the crater (Figure 11a). Estimates of the volatile context excavated by the impact are up to 1.9×10^{12} m^3, assuming that 10% of the subsurface pore volume was ice (Jones et al., 2011). Volatiles incorporated into the ejecta would liquefy or vaporize as a result of heating by the surrounding hot ejecta, which for a crater the size of Hale, is estimated to be around ~350 K (Weiss & Head, 2016). The ejecta closer to the crater was likely to be hotter than average, as it was thicker and had less time to cool during travel. Correspondingly, the more distal deposits would be cooler due to being thinner and traveling for longer (Figure 11a). Initially, not all the pore spaces within the ejecta would have been filled by volatiles, but over time saturation of the ejecta took place. This may have occurred due to continued melting of

volatiles within the ejecta or contraction of the ejecta as it settled, leading to pore spaces being closed and the remaining pore spaces being occupied to the point of saturation (Morino et al., 2019).

In some locations, the saturated ejecta transitioned into a flowing mass analogous to a debris flow (Figure 11b), and the topography influenced the movement of the ejecta across the study site (Carr et al., 1977). This is particularly evident in HCV 1, HCV 2, and the LWLD, where the ejecta was channelized into the valleys and flowed downslope. The presence of marginal deposits stranded upon the valley sides along HCV 2 (Figures 7c and 7d) and LWLD (Figure 10e) records the former height of the ejecta flows down the valleys (Figure 11b), similar to terrestrial debris flows (Crandell, 1971). This occurred within hours or days for both the proximal and distal deposits, despite their different emplacement mechanisms, as isolated marginal deposits are also present in the distal deposits from Hale crater (Grant & Wilson, 2018). As the ejecta material flowed across the landscape, the finer and more liquefied portions drained around more boulder-rich and blocky parts of the flow. As the carrying capacity of the flow decreased, the blocky sections were emplaced more easily, and the finer material continued to drain around them, exposing the mounds.

Ultimately, the flows of ejecta terminated in the Eastern Basin or the Western Basin. The lobate shape of the downstream ejecta deposits in HCV 2 and the Eastern Basin (Figures 7e and 9) marks where some of the flows of ejecta terminated (Figure 11b). Debris flows and other mass flow deposits exhibit these characteristic lobate shapes (Christiansen, 1989; Voight et al., 1983) as they possess high yield strength and cohesiveness due to friction between grains in the flow (Cronin et al., 1997). These lobate planform appearances are limited to certain parts of the ejecta blanket, indicating that not all of the ejecta behaved in this manner, and there is no evidence for arcuate ridges (Grant & Wilson, 2018) or multiple lobes (Christiansen, 1989) on the surfaces of the ejecta within HCV 1 or 2, suggesting that only one flow event occurred in these valleys. However, the differing morphologies of their terminal regions suggest that these flows may not have occurred at the same time. Eventually, the movement of the ejecta ceased or slowed dramatically, and water that remained in the pore spaces of the ejecta was evacuated and incised the ejecta surface producing the linear depressions (Figure 11c). The formation of the linear depressions would have taken place before the deposits froze entirely, and so would have been limited by how long it took for the ejecta to cool. Calculations of ejecta cooling rates suggest that the ejecta would have remained hot enough to melt liquid water for at least hundreds of years and potentially up to tens of thousands of years (Weiss & Head, 2016). The linear depressions likely formed not long after the ejecta was deposited, as they are located within comparatively thin ejecta at the margins of the continuous ejecta zone, which would have cooled faster to ambient temperatures than thicker ejecta closer to the crater (Weiss & Head, 2016). This is particularly true of the Type 1 linear depressions, which are located at the very fringes of the ejecta lobes.

Following the cessation of fluvial activity, the polygons formed. Broadly, it is likely these polygons formed not long after the mounds and linear depressions, as the polygons are also located at the comparatively thin and rapidly cooled ejecta margins. Changes to the local climate could initiate further polygon development (Levy et al., 2009), and this is possible in one billion year since Hale crater formed. However, the most simplistic solution is that the polygons are related to the impact and not to possible later climate variations. Therefore, the majority of the landforms described in this work likely reflect the behavior and evolution of the ejecta in the weeks, months, and possibly years immediately following the impact, rather than processes spread out over a longer geological time period.

6. Conclusions

In this study, we describe a suite of landforms within the Hale crater ejecta not previously noted in detail, and we have described in the evolution of the ejecta and the creation of these landforms. Our main finding is that the Hale crater ejecta contained volatiles and these facilitated the development of this suite of landforms through significant geomorphic and aqueous activity, in line with previous study (El-Maarry et al., 2013; Grant & Wilson, 2018; Jones et al., 2011). Overall, we suggest that the ejecta proximal to Hale crater was emplaced and evolved in a sequence of events that is similar to many crater ejecta blankets on Mars, such as Tooting (Morris et al., 2010), Bamburg (Mouginis-Mark, 1979), and Bakyhausen (Caudill et al., 2018). Principally, that the ejecta morphologies and landforms present in the study site formed in a phase of activity beginning immediately after the majority of the ejecta had been initially deposited and secondary crater impacts had occurred (Grant & Wilson, 2018). We also interpret the Hale ejecta deposits to

reveal a complex and diverse evolution that was spatially variable, with concentrated dewatering and surface flow occurring, the formation of polygons, and the production of potentially unique mound features. Despite the evidence for the release of surface water from the ejecta, the geomorphology suggests that this was short-lived and spatially restricted making it of limited use for biology.

The similar bulk ejecta morphology between the study site, Moanda crater system, and the Hale crater distal deposits indicates that the volatile content of the ejecta material was broadly consistent between the distal deposits and proximal deposits (Grant & Wilson, 2018). However, this work also highlights that the volatile content of the ejecta was spatially variable on smaller scales and changed over time, which may indicate that the topography influenced how the presence of volatiles was expressed at the surface. Examples of this variation include the lack of mounds noted in the deposits far from Hale crater, the differences between the terminal deposits in HCV 1 and HCV 2, the downstream changes in the geometry of the LWLD and the limited locations of the polygon features. These variations mean that care should be taken when using these landforms to infer volatile content of the subsurface and entire ejecta blanket, as while the ejecta material as a whole appears to have a broadly similar volatile content, the landforms within and upon it are not consistent across the ejecta in the same way.

Data Availability Statement

The data sources utilized in this study can be accessed at the following locations: MOLA (https://astrogeology.usgs.gov/search/map/Mars/GlobalSurveyor/MOLA/Mars_MGS_MOLA_DEM_mosaic_global_463m) and THEMIS (https://astrogeology.usgs.gov/search/map/Mars/Odyssey/THEMIS-IR-Mosaic-ASU/Mars_MO_THEMIS-IR-Day_mosaic_global_100m_v12). CTX data are available through the NASA Planetary Data System (https://pds.nasa.gov/). HiRISE data can be accessed through the University of Arizona (at https://hirise.lpl.arizona.edu/). HRSC data are available online (at http://hrscview.fu-berlin.de/). Finally, the shapefiles and HiRISE DEM created in this study can be accessed at Zenodo (https://doi.org/10.5281/zenodo.3888220).

Acknowledgments

This work was supported by an M.Phil. bursary and a Research Excellence Academy PhD Studentship awarded to J. L. Collins-May, from the School of Geography, Politics and Sociology, Newcastle University. We thank A. Large and S. J. Conway for their comments through the M.Phil. submission process. We also thank P. Mouginis-Mark, D. Viola, and an anonymous reviewer for their comments and suggestions, which greatly improved the paper. Finally, we would like to thank F. E. G. Butcher at the Open University for the training in HiRISE DEM production.

References

Abramov, O., & Kring, D. A. (2004). Numerical modeling of an impact-induced hydrothermal system at the Sudbury crater. *Journal of Geophysical Research*, *109*, E10007. https://doi.org/10.1029/2003JE002213

Abramov, O., & Kring, D. A. (2005). Impact-induced hydrothermal activity on early Mars. *Journal of Geophysical Research*, *110*, E12S09. https://doi.org/10.1029/2005JE002453

Balme, M., Berman, D. C., Bourke, M. C., & Zimbelman, J. R. (2008). Transverse aeolian ridges (TARs) on Mars. *Geomorphology*, *101*(4), 703–720. https://doi.org/10.1016/j.geomorph.2008.03.011

Barlow, N. G., & Perez, C. B. (2003). Martian impact crater ejecta morphologies as indicators of the distribution of subsurface volatiles. *Journal of Geophysical Research*, *108*(E8), 5085. https://doi.org/10.1029/2002JE002036

Boynton, W. V., Feldman, W. C., Squyres, S. W., Prettyman, T. H., Bruckner, J., Evans, L. G., et al. (2002). Distribution of hydrogen in the near surface of Mars: Evidence for subsurface ice deposits. *Science*, *297*(5578), 81–85. https://doi.org/10.1126/science.1073722

Brooker, L. M., Balme, M. R., Conway, S. J., Hagermann, A., Barrett, A. M., Collins, G. S., & Soare, R. J. (2018). Clastic polygonal networks around Lyot crater, Mars: Possible formation mechanisms from morphometric analysis. *Icarus*, *302*, 386–406. https://doi.org/10.1016/j.icarus.2017.11.022

Byrne, S., Dundas, C. M., Kennedy, M. R., Mellon, M. T., McEwen, A. S., Cull, S. C., et al. (2009). Distribution of mid-latitude ground ice on mars from new impact craters. *Science*, *325*(5948), 1674–1676. https://doi.org/10.1126/science.1175307

Carr, M. H., Crumpler, L. S., Cutts, J. A., Greeley, R., Guest, J. E., & Masursky, H. (1977). Martian impact craters and emplacement of ejecta by surface flow. *Journal of Geophysical Research*, *82*(28), 4055–4065. https://doi.org/10.1029/JS082i028p04055

Carr, M. H. (1987). Water on Mars. *Nature*, *326*(6108), 30–35. https://doi.org/10.1038/326030a0

Caudill, C. M., Osinski, G. R., & Tornabene, L. L. (2018). Ejecta deposits of Bakhuysen Crater, Mars. *Icarus*, *314*, 175–194. https://doi.org/10.1016/j.icarus.2018.06.001

Christiansen, E. H. (1989). Lahars in the Elysium region of Mars. *Geology*, *17*(3), 203–206. https://doi.org/10.1130/0091-7613(1989)017%3C0203:LITERO%3E2.3.CO;2

Costard, F. M., & Kargel, J. S. (1995). Outwash plains and thermokarst on mars. *Icarus*, *114*(1), 93–112. https://doi.org/10.1006/icar.1995.1046

Craddock, R. A., & Howard, A. D. (2002). The case for rainfall on a warm, wet early Mars. *Journal of Geophysical Research*, *107*(E11), 5111. https://doi.org/10.1029/2001JE001505

Crandell, D. R. (1971). Postglacial lahars from Mount Rainer Volcano, Washington. *Geological Survey Professional Paper*, *667*, 1–75.

Cronin, S. J., Neall, V. E., & Palmer, A. S. (1997). Lahar history and hazard of the Tongariro River, northeastern Tongariro Volcanic Centre, New Zealand. *New Zealand Journal of Geology and Geophysics*, *40*(3), 383–393. https://doi.org/10.1080/00288306.1997.9514769

Dohm, J. M., Hare, T. M., Robbins, S. J., Williams, J. P., Soare, R. J., el-Maarry, M. R., et al. (2015). Geological and hydrological histories of the Argyre province, Mars. *Icarus*, *253*, 66–98. https://doi.org/10.1016/j.icarus.2015.02.017

Dundas, C. M., Bramson, A. M., Ojha, L., Wray, J. J., Mellon, M. T., Byrne, S., et al. (2018). Exposed subsurface ice sheets in the Martian mid-latitudes. *Science*, *359*(6372), 199–201. https://doi.org/10.1126/science.aao1619

El-Maarry, M. R., Dohm, J. M., Michael, G., Thomas, N., & Maruyama, S. (2013). Morphology and evolution of the ejecta of Hale crater in Argyre basin, Mars: Results from high resolution mapping. *Icarus*, *226*(1), 905–922. https://doi.org/10.1016/j.icarus.2013.07.014

Fanale, F. P., Salvail, J. R., Zent, A. P., & Postawko, S. E. (1986). Global distribution and migration of subsurface ice on mars. *Icarus*, *67*(1), 1–18. https://doi.org/10.1016/0019-1035(86)90170-3

Feldman, W. C., Boynton, W. V., Tokar, R. L., Prettyman, T. H., Gasnault, O., Squyres, S. W., et al. (2002). Global distribution of neutrons from Mars: Results from Mars Odyssey. *Science*, *297*(5578), 75–78. https://doi.org/10.1126/science.1073541

Goddard, K., Warner, N. H., Gupta, S., & Kim, J.-R. (2014). Mechanisms and timescales of fluvial activity at Mojave and other young Martian craters. *Journal of Geophysical Research: Planets*, *119*, 604–634. https://doi.org/10.1002/2013JE004564

Grant, J. A., & Parker, T. J. (2002). Drainage evolution in the Margaritifer Sinus region, Mars. *Journal of Geophysical Research*, *107*(E9), 5066. https://doi.org/10.1029/2001JE001678

Grant, J. A., & Wilson, S. A. (2018). The nature and emplacement of distal aqueous-rich ejecta deposits from Hale crater, Mars. *Meteoritics and Planetary Science*, *53*(4), 839–856. https://doi.org/10.1111/maps.12843

Iverson, R. M. (1997). The physics of debris flows. *Reviews of Geophysics*, *35*(3), 245–296. https://doi.org/10.1029/97RG00426

Jaumann, R., Neukum, G., Behnke, T., Duxbury, T. C., Eichentopf, K., Flohrer, J., et al. (2007). The high-resolution stereo camera (HRSC) experiment on Mars Express: Instrument aspects and experiment conduct from interplanetary cruise through the nominal mission. *Planetary and Space Science*, *55*(7–8), 928–952. https://doi.org/10.1016/j.pss.2006.12.003

Jaumann, R., Tirsch, D., Hauber, E., Ansan, V., di Achille, G., Erkeling, G., et al. (2015). Quantifying geological processes on Mars—Results of the High Resolution Stereo Camera (HRSC) on Mars Express. *Planetary and Space Science*, *112*, 53–97. https://doi.org/10.1016/j.pss.2014.11.029

Johnson, C. G., Kokelaar, B. P., Iverson, R. M., Logan, M., LaHusen, R. G., & Gray, J. M. N. T. (2012). Grain-size segregation and levee formation in geophysical mass flows. *Journal of Geophysical Research*, *117*, F01032. https://doi.org/10.1029/2011JF002185

Jones, A. P., McEwen, A. S., Tornabene, L. L., Baker, V. R., Melosh, H. J., & Berman, D. C. (2011). A geomorphic analysis of Hale crater, Mars: The effects of impact into ice-rich crust. *Icarus*, *211*(1), 259–272. https://doi.org/10.1016/j.icarus.2010.10.014

Kadish, S. J., Head, J. W., Barlow, N. G., & Marchant, D. R. (2008). Martian pedestal craters: Marginal sublimation pits implicate a climate-related formation mechanism. *Geophysical Research Letters*, *35*, L16104. https://doi.org/10.1029/2008GL034990

Kirk, R. L., Howington-Kraus, E., Rosiek, M. R., Anderson, J. A., Archinal, B. A., Becker, K. J., et al. (2009). Ultrahigh resolution topographic mapping of Mars with MRO HiRISE stereo images: Meter-scale slopes of candidate Phoenix landing sites. *Journal of Geophysical Research*, *113*, E00A24. https://doi.org/10.1029/2007JE003000

Kress, A. M., & Head, J. W. (2008). Ring-mold craters in lineated valley fill and lobate debris aprons on Mars: Evidence for subsurface glacial ice. *Geophysical Research Letters*, *35*, L23206. https://doi.org/10.1029/2008GL035501

Levy, J., Head, J., & Marchant, D. (2009). Thermal contraction crack polygons on Mars: Classification, distribution, and climate implications from HiRISE observations. *Journal of Geophysical Research*, *114*, E01007. https://doi.org/10.1029/2008JE003273

MacPhail, D. D. (1973). The geomorphology of the Rio Teno lahar, Central Chile. *Geographical Review*, *63*(4), 517. https://doi.org/10.2307/213919

Major, J. J., & Iverson, R. M. (1999). Debris-flow deposition: Effects of pore-fluid pressure and friction concentrated at flow margins. *Geological Society of America Bulletin*, *111*(10), 1424–1434. https://doi.org/10.1130/0016-7606(1999)111<1424:dfdeop>2.3.co;2

Malin, M. C., Bell, J. F. III, Cantor, B. A., Caplinger, M. A., Calvin, W. M., Clancy, R. T., et al. (2007). Context Camera Investigation on board the Mars Reconnaissance Orbiter. *Journal of Geophysical Research*, *112*, E05S04. https://doi.org/10.1029/2006JE002808

Mangold, N., Maurice, S., Feldman, W. C., Costard, F., & Forget, F. (2004). Spatial relationships between patterned ground and ground ice detected by the neutron spectrometer on Mars. *Journal of Geophysical Research*, *109*, E08001. https://doi.org/10.1029/2004JE002235

McEwen, A. S., Eliason, E. M., Bergstrom, J. W., Bridges, N. T., Hansen, C. J., Delamere, W. A., et al. (2007). Mars reconnaissance orbiter's High Resolution Imaging Science Experiment (HiRISE). *Journal of Geophysical Research*, *112*, E05S02. https://doi.org/10.1029/2005JE002605

Mellon, M. T., Arvidson, R. E., Sizemore, H. G., Searls, M. L., Blaney, D. L., Cull, S., et al. (2009). Ground ice at the Phoenix landing site: Stability state and origin. *Journal of Geophysical Research*, *114*, E00E07. https://doi.org/10.1029/2009JE003417

Morgan, G. A., & Head, J. W. III (2009). Sinton crater, Mars: Evidence for impact into a plateau icefield and melting to produce valley networks at the Hesperian-Amazonian boundary. *Icarus*, *202*(1), 39–59. https://doi.org/10.1016/j.icarus.2009.02.025

Morino, C., Conway, S. J., Balme, M. R., Hillier, J., Jordan, C., Saemundsson, Þ., & Argles, T. (2019). Debris-flow release processes investigated through the analysis of multi-temporal LiDAR datasets in north-western Iceland. *Earth Surface Processes and Landforms*, *44*(1), 144–159. https://doi.org/10.1002/esp.4488

Morris, A. R., Mouginis-Mark, P. J., & Garbeil, H. (2010). Possible impact melt and debris flows at Tooting Crater, Mars. *Icarus*, *209*(2), 369–389. https://doi.org/10.1016/j.icarus.2010.05.029

Mouginis-Mark, P. J. (1987). Water or ice in the Martian regolith?: Clues from rampart craters seen at very high resolution. *Icarus*, *71*(2), 268–286. https://doi.org/10.1016/0019-1035(87)90152-7

Mouginis-Mark, P. J. (1979). Ejecta emplacement of the Martian impact crater Bamburg. *Lunar and Planetary Science Conference, 10th*, *3*, 2651–2668.

Picardi, G., Plaut, J. J., Biccari, D., Bombaci, O., Calabrese, D., Cartacci, M., et al. (2005). Planetary science: Radar soundings of the subsurface of Mars. *Science*, *310*(5756), 1925–1928. https://doi.org/10.1126/science.1122165

Putzig, N. E., Phillips, R. J., Campbell, B. A., Mellon, M. T., Holt, J. W., & Brothers, T. C. (2014). SHARAD soundings and surface roughness at past, present, and proposed landing sites on Mars: Reflections at Phoenix may be attributable to deep ground ice. *Journal of Geophysical Research: Planets*, *119*, 1936–1949. https://doi.org/10.1002/2014JE004646

Schultz, P. H., & Wrobel, K. E. (2012). The oblique impact Hale and its consequences on Mars. *Journal of Geophysical Research*, *117*, E04001. https://doi.org/10.1029/2011JE003843

Seu, R., Phillips, R. J., Biccari, D., Orosei, R., Masdea, A., Picardi, G., et al. (2007). SHARAD sounding radar on the Mars Reconnaissance Orbiter. *Journal of Geophysical Research*, *112*, E05S05. https://doi.org/10.1029/2006JE002745

Siebert, L. (1984). Large volcanic debris avalanches: Characteristics of source areas, deposits, and associated eruptions. *Journal of Volcanology and Geothermal Research*, *22*(3–4), 163–197. https://doi.org/10.1016/0377-0273(84)90002-7

Smith, D. E., Zuber, M. T., Frey, H. V., Garvin, J. B., Head, J. W., Muhleman, D. O., et al. (2001). Mars Orbiter Laser Altimeter: Experiment summary after the first year of global mapping of Mars. *Journal of Geophysical Research*, *106*(E10), 23,689–23,722. https://doi.org/10.1029/2000JE001364

Soare, R. J., Conway, S. J., & Dohm, J. M. (2014). Possible ice-wedge polygons and recent landscape modification by "wet" periglacial processes in and around the Argyre impact basin, Mars. *Icarus*, *233*, 214–228. https://doi.org/10.1016/j.icarus.2014.01.034

Soare, R. J., Osinski, G. R., & Roehm, C. L. (2008). Thermokarst lakes and ponds on Mars in the very recent (late Amazonian) past. *Earth and Planetary Science Letters*, *272*(1–2), 382–393. https://doi.org/10.1016/j.epsl.2008.05.010

Turner, S. M. R., Bridges, J. C., Grebby, S., & Ehlmann, B. L. (2016). Hydrothermal activity recorded in post Noachian-aged impact craters on Mars. *Journal of Geophysical Research: Planets*, *121*, 608–625. https://doi.org/10.1002/2015JE004989

Vijayan, S., Sinha, R. K., Harish, & Anilkumar, R. (2020). Evidence for Multiple Superposed Fluvial Deposits Within Reuyl Crater, Mars. *Journal of Geophysical Research: Planets*, *125*(3). https://doi.org/10.1029/2019JE006136

Voight, B., Janda, R. J., Glicken, H., & Douglass, P. M. (1983). Nature and mechanics of the Mount St Helens rockslide-avalanche of 18 May 1980. *Geotechnique*, *33*(3), 243–273. https://doi.org/10.1680/geot.1983.33.3.243

Weiss, D. K., Head, J. W., Palumbo, A. M., & Cassanelli, J. P. (2017). Extensive Amazonian-aged fluvial channels on Mars: Evaluating the role of Lyot crater in their formation. *Geophysical Research Letters*, *44*, 5336–5344. https://doi.org/10.1002/2017GL073821

Weiss, D. K., & Head, J. W. (2013). Formation of double-layered ejecta craters on Mars: A glacial substrate model. *Geophysical Research Letters*, *40*, 3819–3824. https://doi.org/10.1002/grl.50778

Weiss, D. K., & Head, J. W. (2016). Impact ejecta-induced melting of surface ice deposits on Mars. *Icarus*, *280*, 205–233. https://doi.org/10.1016/j.icarus.2016.07.007

Whelley, P. L., Jay, J., Calder, E. S., Pritchard, M. E., Cassidy, N. J., Alcaraz, S., & Pavez, A. (2012). Post-depositional fracturing and subsidence of pumice flow deposits: Lascar Volcano, Chile. *Bulletin of Volcanology*, *74*(2), 511–531. https://doi.org/10.1007/s00445-011-0545-1

Williams, R. M. E., & Malin, M. C. (2008). Sub-kilometer fans in Mojave Crater, Mars. *Icarus*, *198*(2), 365–383. https://doi.org/10.1016/j.icarus.2008.07.013

Wilson, L., Ghatan, G. J., Head, J. W. III, & Mitchell, K. L. (2004). Mars outflow channels: A reappraisal of the estimation of water flow velocities from water depths, regional slopes, and channel floor properties. *Journal of Geophysical Research*, *109*, E09003. https://doi.org/10.1029/2004JE002281